이학석사 학위논문

고지방식이에 의한 대장 줄기세포 조절 연구

Control of colonic stem cells and their niche by high-fat-diet

울산대학교 대학원

의 학 과

김 태 영

Control of colonic stem cells and their niche by high-fat-diet

지 도 교 수　권 미 나

이 논문을 이학석사학위 논문으로 제출함

2019 년 8 월

울산대학교 대학원

의 학 과

김 태 영

김태영의 이학석사학위 논문을 인준함

심사위원 예 병 덕 (인)

심사위원 박 윤 용 (인)

심사위원 권 미 나 (인)

울 산 대 학 교 대 학 원

2019 년 8 월

Abstract

Dietary signals are known to modulate stemness and tumorigenicity of intestinal progenitors. Previous other studies demonstrated that high-fat-diet (HFD) enhanced numbers of $Lgr5^+$ intestinal stem cells (ISCs) and further promoted primary and metastatic colon cancer. However, little is known how HFD-induced obesity affects ISC niche which might be involved in initiation of colorectal cancer. Understanding their effects will provide the mechanism about the risk factors of HFD-induced colorectal cancer. In this study, we found that histopathological scores were enhanced in the colon of HFD-fed mice in comparison to those of purified diet (PD)-fed one in a steady state. We confirmed that HFD feeding resulted in highly enhanced susceptibility to AOM-DSS-induced colorectal cancer. Although no significant changes of ISC numbers were addressed in the colon of HFD-fed mice, $Ki67^+$ proliferating cells were significantly increased in the proximal and distal regions. Since deep crypt secretory cells, one of the niches supporting ISC maintenance in the colon, were not altered by HFD feeding, we next focused on the function of colon mesenchymal stromal cells (MSCs). Compared to those from PD-fed mice, colonic MSCs isolated from HFD-fed mice enhanced the growth of organoid derived from normal and malignant colon. The fact that Wnt2b secretion by colon PDGFR-α^+ MSCs was significantly higher in HFD-fed mice than those in PD-fed mice, indicating that MSCs might play a crucial role on tumorigenesis in the colon of obese mice. Metagenomic analysis showed that decreased diversity of resident gut bacteria were found in the feces of HFD-fed mice when compared with those from PD-fed mice. Levels of free-fatty-acid (FFA) in the cecal contents were increased in HFD-fed mice compared to PD-fed mice while no differences of short chain fatty acid were revealed. Furthermore, FFA was indispensable factor to promote colon organogenesis. Taken together, these results demonstrate that colon PDGFR-α^+ MSCs and FFA might be critically involved on modulation of intestinal cancer stem cells in HFD-induced obesity.

Keywords: HFD; colon cancer; ISCs; MSCs

Contents

List of Figures

Introduction

1. Intestinal stem cells and cancer stem cells

The intestinal epithelium is known as the most rapidly self-renewing tissue every 4 to 5 days [1, 2]. Intestinal epithelial cells are generated in crypts, migrate rapidly toward the surface, and die at the tip of finger-like protrusions known as villi where cell loss is compensated by constant cell production in crypts. These rapid cellular turnover of the intestine tissue is promoted by Leucine-rich-repeat-containing G-protein-coupled receptor 5 (Lgr5) expressing intestinal stem cells (ISCs) existing in the bottom of crypts [3] and Lgr5 acts as a receptor for R-spondins which potent Wnt signal enhancers and growth factors of ISCs [4]. $Lgr5^+$ ISCs are actively proliferating cells and they give rise to progenitors that can differentiate into the various mature epithelial cells such as enterocytes, goblet cells, enteroendocrine cells, and Paneth cells. The cells with terminal differentiation are generated by amplification of the progenitor pool through several rounds of cell division before differentiation [5]. On the other hands, role of $Lgr5^+$ ISCs as cancer-initiating stem cells in the colorectal cancer has been reported [6, 7]. Ablation of $Lgr5^+$ cells in mice does not suppress colorectal cancers, but these cells are critical for liver metastasis from colorectal cancers [7]. However, there is still lack of experimental evidence as to the functional relevance of cancer stem cells (CSCs) such as $Lgr5^+$ cells in colorectal cancers. It is also required to study which factors transform normal stem cell into CSCs.

2. Intestinal stem cell niche

ISC niche not only maintain intestine epithelial homeostasis but also control proliferation and differentiation of ISCs through variety of signaling pathways. The ISC niche is composed of a cellular part and a physical part. There are Paneth cells and mesenchymal stromal cells (MSCs) in the cellular ISC niche in the small intestine. Paneth cells are located between ISCs and progenitor parts in intestinal crypt region and known to supply Wnt3, epidermal growth factor (EGF), and Notch ligands [8, 9]. Our recent study suggested that αSMA^+ stromal cells in the small intestine supported ISCs-mediated epithelial differentiation [10].

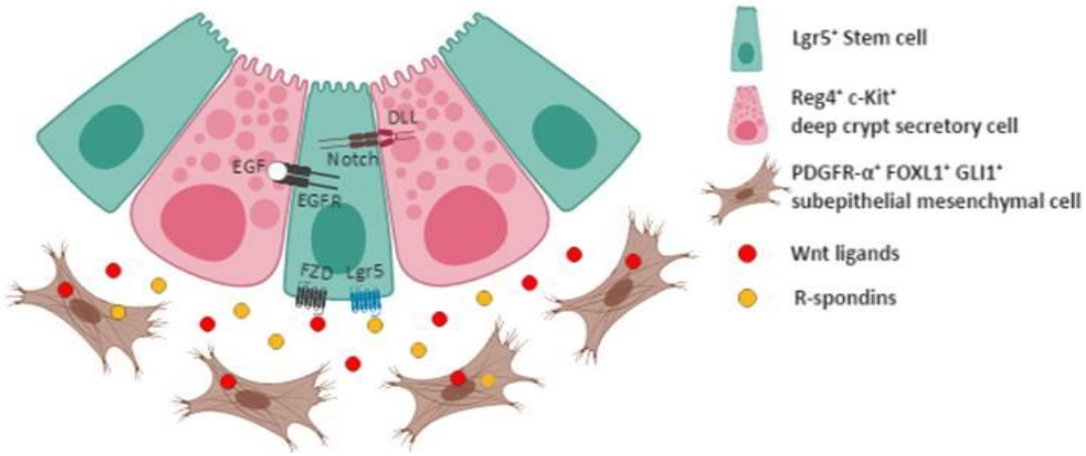

Figure 1. Intestinal stem cell niche in the colon. Lgr5 intestinal stem cells (ISCs) were supported through signaling molecules provided by ISC niche. Reg4^{+} c-Kit^{+} deep crypt secretory cells provide ISCs with EGF and Notch ligands for stemness, subepithelial mesenchymal stromal cell (MSC)-derived Wnt ligands and R-spondins enhance the proliferative activation of ISCs. Image was created with BioRender.com.

In case of colon which does not possess Paneth cells, deep crypt secretory (DCS) cells are proposed as one of ISC niche [9, 11]. MSCs as connective-tissue cells secrete indispensable signaling molecules and growth factors to maintain ISCs homeostasis [12-14]. As like as Paneth cells in the small intestine, Reg4^{+} DCS cells in the colon are intermingled with colonic stem cells at bottom of crypt regions by providing EGF and Notch ligands [11]. Of interest, DCS cells do not produce the Wnt ligands, whereas Paneth cells produce high levels of Wnt3 [11]. Nonetheless, colonic stem cells express Wnt receptors because colonic MSCs surrounding crypts provide Wnt ligands (i.e., Wnt2b, Wnt4 and Wnt5a) [11, 12]. The physical ISC niche indicates the extracellular matrix (ECM) components secreted by MSCs which maintaining ISC homeostasis through biochemical and mechanical signals [15].

3. Intestinal mesenchymal stromal cells

The intestinal MSCs are composed of various cell types such as stromal cells (telocytes), fibroblasts, and smooth muscle cells [16, 17]. MSCs are located within the lamina propria in close proximity to the ISCs and crypt–villus junction [17, 18]. MSCs are known to provide signaling molecules such as Wnt ligands and R-spondins in the stromal niche for ISCs maintenance [12-14] and improve intestinal epithelial repair by injury [19, 20]. Recent study

suggested that FOXL1-expressing telocytes are an important source of producing Wnt ligands [17] and subepithelial MSCs expressing GLI1 are an essential ISC niche providing Wnt ligands [21]. In addition, both $FOXL1^+$ or $GLI1^+$ MSCs that secrete Wnt ligands commonly express platelet-derived growth factor receptor-α (PDGFR-α) [17, 21]. Although MSCs support maintenance of ISCs, they have duplicity in that they contribute to cancer development [22]. Cancer-associated fibroblasts in tumor microenvironment promote tumor development and progression through secretion of cytokines, growth factors, and ECM. We therefore speculate that MSCs play an indispensable role to control colonic stem cells and CSCs.

4. Wnt signaling pathway

Wnt signaling is essential for both stem cell maintenance and tissue regeneration in the adult organism. However, ectopic Wnt signaling causes variety of cancers and promotes tumor progression [23-25]. In particular, ectopic Wnt signaling in the $Lgr5^+$ ISCs promote the progression of intestinal tumors [6] and increase the proliferation and invasion of gastric adenocarcinoma cells [26]. Wnt signaling are classified as β-catenin dependent pathway (canonical) and β-catenin independent pathway (non-canonical) [23, 27]. Cancer is often initiated by mutations on downstream of the Wnt receptor complex, whereas Wnt ligand is important for the proliferation and survival of colon cancer cells [28]. Importantly, Wnt2b, one of the Wnt ligands, is known to be highly overexpressed from fibroblasts in the tumor microenvironment [23]. In the process of Wnt secretion, all Wnt proteins undergo lipid modification in which palmitate is attached by palmitoyltransferase Porcupine residing in endoplasmic reticulum (ER) [24]. Thereafter, the transmembrane protein Wntless (Wls) binds only lipid-modified Wnt proteins and transports them to the plasma membrane to secrete. When the secreted Wnt ligands arrive at the target cells, Wnt ligands bind to their cognate Frizzled receptors through their palmitic acid group. Wnt ligands then bind to the low-density-lipoprotein related receptor 5 and 6 (LRP5/6) co-receptor and form a complex with Frizzled, followed by an increase in translocation of β-catenin to nuclear [24].

5. Increased tumorigenesis by high-fat-diet

Previous studies demonstrated that Lgr5^{+} ISCs are affected by dietary signals and remodel the composition of intestinal epithelium [29-31]. Self-renewal and differentiation of Lgr5^{+} ISCs can be regulated through cell-autonomous and non-autonomous mechanisms in response to dietary signals [29, 31, 32]. For instance, high-fat-diet (HFD) is known to directly increase the function of ISCs and progenitors [32]. On the other hand, as an example of a non-autonomous mechanism, calorie restriction enhances the function of ISCs by affecting neighboring Paneth cells [29, 31]. However, it is still unclear how ISCs niche respond to dietary signals. There have been many reports that obesity increases colon cancer incidence [30, 33]. Especially, HFD-induced obesity is known to induce a low-grade inflammatory state [34, 35] and increase the potential to initiate tumors in the intestine [30, 32]. In contrast, genetically modified obesity model [i.e., leptin receptor deficient (db/db) mice] was opposite to phenotype in HFD-induced obesity [32]. HFD enhances the numbers and functions of Lgr5^{+} ISCs directly through a peroxisome proliferator activated receptor-delta (PPAR-δ) signaling that activated by fatty acid [30, 32]. Of note, activated PPAR-δ signaling from HFD amplifies canonical Wnt signaling in ISCs and progenitor cells, and in vivo PPAR-δ agonist treatment increase the capability to initiate tumors from intestinal progenitor cells [32].

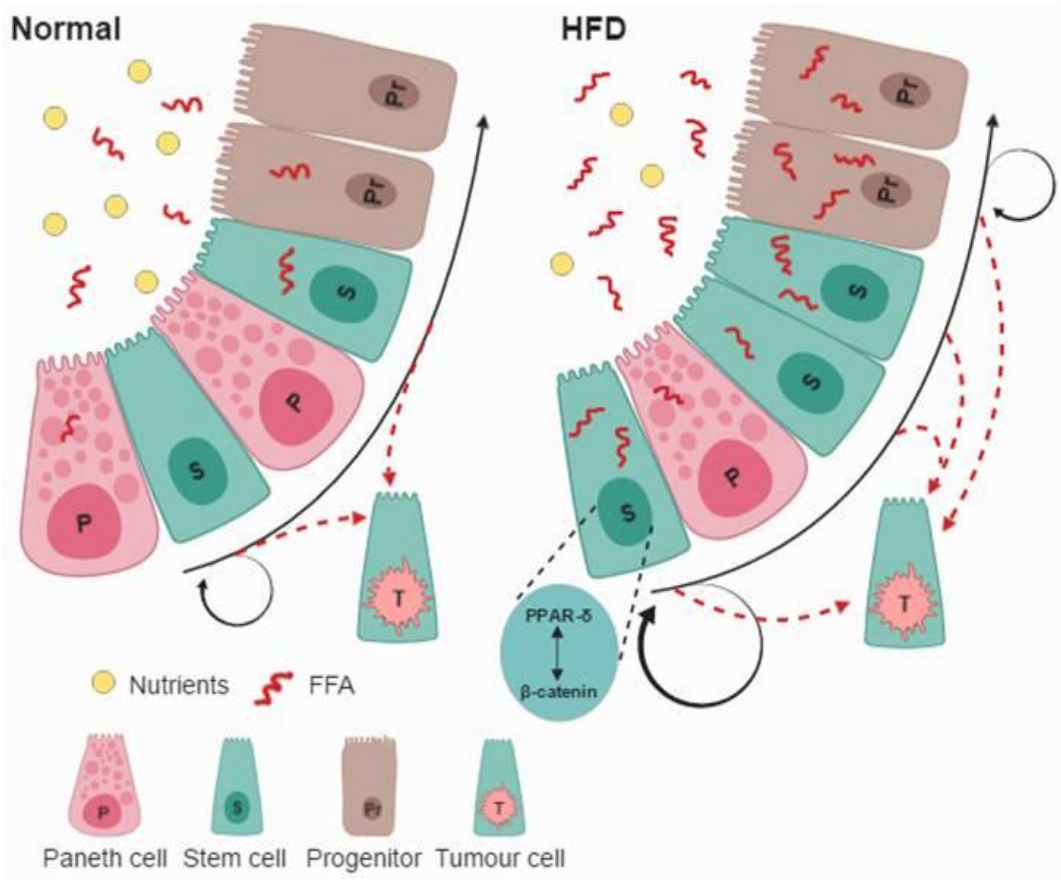

Figure 2. Intestinal tumorigenesis increased by HFD. In the intestine, FFA increased by HFD promotes binding to nuclear PPAR-δ in ISCs and progenitors. PPAR-δ signaling activated by FFA binding stimulates β-catenin target genes by β-catenin translocation to the nucleus. Activated β-catenin target genes increase the numbers and function of ISCs. Notably, HFD endows regenerative capacity to progenitors, and enforces the progenitors to transform into tumor cells. Image was created with BioRender.com.

6. The Rationale of my study

As reported by others, we confirmed in this study that HFD feeding more likely to give rise to colon cancer. Since MSCs are a component of tumor microenvironment that supports stemness and tumorigenecity of ISCs, we aimed to investigate an exact role of MSCs on the colon cancer in HFD-induced obesity.

Material and Methods

Mice and diet.

C57BL/6N mice were purchased from Orient Bio (South Korea), and Lgr5-EGFP-IRES-CreERT2 mice and C57BL/6J-$Apc^{Min/+}$ mice were purchased from Jackson Laboratory (Bar Harbor, ME), respectively. All mice were housed under specific pathogen-free conditions in the animal facility at Asan Medical Center, where they received water ad libitum. Three diets were used during experiment; standard normal chow (Purina 5057, Purina), PD (D10012G, Research Diets), and HFD (D12492, Research Diets), and mice received diets ad libitum beginning at the age of 8-10 weeks and extending for at least 3 months. Mice were sex- and age- matched between groups. $Apc^{Min/+}$ mice with spontaneous intestinal adenoma after housing for 15 weeks were used for colon cancer organoid culture.

Experimental inflammation-induced colorectal cancer model.

Mice were given a single intraperitoneal injection of AOM (12.5 mg/kg body weight, Sigma Aldrich) in combination with three cycles of DSS treatment as illustrated in Figure 5A.

Histology.

Mouse intestines were rolled by the Swiss roll technique and fixed in 4% paraformaldehyde (PFA) and embedded in paraffin. The paraffin-embedded blocks were cut into 5 μm sections and stained with hematoxylin-eosin (H&E) or periodic acid-Schiff (PAS). For the PAS staining, tissue section-slides were deparaffinized and rehydrated and placed in 1% periodic acid solution at RT for 5 min. Slides were then washed and immersed in Schiff's reagent for 15 min and stained with hematoxylin.

Histological scoring.

Histological grade was scored by blinded investigators through a scoring system as described previously [36]: severity of inflammation (0, none; 1, slight; 2, moderate; 3, severe), extent of injury (0, none; 1, mucosa; 2, mucosa and submusoca; 3, transmural and epithelium lost), and crypt damage (0, none; 1,basal one-third damaged; 2, basal two-thirds damaged; 3, only

surface epithelium intact; 4, entire crypt and epithelium lost). Finally, these indicators were also quantified as to the percentage involvement by the disease conditions (0, 0%-25%; 1, 26%-50%, 2, 51%-75%; 3, 76%-100%).

Immunofluorescence staining.

Tissue samples were embedded in frozen section compound and paraffin. Paraffin-embedding method was described above. For the frozen section, mouse intestines were rolled by the Swiss roll technique and fixed in 4% paraformaldehyde (PFA) and embedded in paraffin. The paraffin-embedded blocks were cut into 5 μm sections. Intestine tissues were fixed with 4% PFA and dehydrated stepwise with 15% and 30% sucrose in PBS. Dehydrated tissues were rolled by the Swiss roll technique. Thereafter, rolled tissues were then embedded in OCT compound (Sakura Finetek), frozen, sliced to 5 μm and tissue sections were fixed in −20°C acetone for 5 min. Paraffin or cryosections were permeabilized in PBS containing 0.5% Triton X-100 at RT for 20 min and blocked with 5% BSA in PBS at RT for 1h. Tissue sections were then stained with primary antibodies overnight at 4℃. After washing with PBS, tissue sections were incubated with secondary antibodies at RT for 1 hr, stained with 4′, 6-diamidino-2-phenylindole (DAPI; Thermo Fisher) for 2 min at RT, and mounted with PermaFluor mountant (Thermo Fisher). To analysis immunofluorescence of intestinal MSCs, plated MSCs were fixed with 4% PFA in PBS. After MSCs were washed in PBS, cells were permeabilized in PBS containing 0.5% Triton X-100 at RT for 30min. After staining, fluorescence images of all samples were captured on an LSM 710 confocal microscope (Carl Zeiss). The following antibodies were used for staining: rat anti-Ki67 (clone 11F6, BioLegend), mouse anti-β-catenin (clone 14, BD Biosciences), mouse anti-αSMA (clone 1A4, Abcam), rabbit anti-Wnt2b (clone EPR13386, Abcam), mouse anti-Wnt2b (clone C-2, Santa Cruz Biotechnology), rabbit anti-PDGFR-α (clone EPR22059-270, Abcam), Alexa flour 546-conjugated goat anti-rat IgG (Thermo Fisher), Alexa fluor 488-conjugated goat anti-mouse IgG (Abcam), and Alexa fluor 488-conjugated goat anti-rabbit IgG (Thermo Fisher).

RNA *in situ* hybridization.

Intestine tissues were fixed in 4% PFA and embedded in paraffin, and used for RNA *in situ* hybridization (RNAscope 2.5 HD Detection kit, Advanced Cell Diagnostics) according to manufacturer instructions. Both Wnt2b and Axin2 RNA probes were purchased and hybridized to their target mRNA.

Crypt isolation.

To obtain crypts from the small intestines, fat and adherent connective tissues were removed. Tissues were opened longitudinally, washed with cold PBS without magnesium chloride and calcium by vigorously shaking and cut approximately at 1 cm pieces. Tissue pieces were incubated in PBS containing 1 mM EDTA at 4°C for 30 min and transferred into PBS containing 5 mM EDTA/gentamycin (Gibco) and incubated for 1hr at 4°C as described previously by others [37]. To isolate the intestinal crypts, tissue pieces were washed with PBS and vigorously shaken and filtered by a 70 μm cell strainer (BD Falcon). In the case of the colon, tissue pieces were incubated in PBS containing 20 mM EDTA/gentamycin (Gibco) at 37°C for 30 min.

Culture condition for crypt organoids.

Isolated crypts were counted and embedded (250~350 crypts / well) in Matrigel (Corning). Matrigel containing crypts were plated to 25 μl per well onto a flat bottom 48-well plate (Thermo Fisher) and cultured in ENR medium containing B27 supplement (Thermo Fisher), N2 supplement (Thermo Fisher), N-acetyl cysteine (Sigma Aldrich), EGF (Thermo Fisher), Noggin (R&D Systems), R-spondin-1-contitioned medium, penicillin-streptomycin (pen/strep; Thermo Fisher), Hepes (Gibco), GlutaMAX (Gibco) and advanced DMEM/F12 (Thermo Fisher) as described previously [37]. Colonic crypts were pelleted and resuspended with TrypLE Express (Thermo Fisher) for 15 min at 37°C to dissociate crypts as described previously [38]. Dissociated colonic crypts were counted by hemocytometer and embedded (1~2 x 10^4 cells / well) in Matrigel (Corning). Colonic crypts were cultured in WENR medium containing Wnt3a in ENR medium. Y-27632 (Sigma Aldrich) and Jagged-1 (AnaSpec) were added to WENR medium for 3 days after the start of the culture as described previously [39]. To manipulate the cancer organoids, colonic crypts from $Apc^{Min/+}$ mice were

isolated and cultured in EN medium without Wnt3a and R-spondin-1. Culture medium was changed every 2 to 3 days. Intestinal organoids were mechanically disrupted by pipetting for subculture or further incubated in TrypLE Express at 37°C for 15min.

Measurement of organoid size.

Organoids were randomly photographed using an inverted microscope (Carl Zeiss) and each photo was analyzed using ImageJ software (NIH) to measure the surface area. Organoid perimeters for area measurements were defined manually by automated ImageJ software.

Treatment of fatty acids and cecal contents.

The following fatty acids have been applied to organoids: palmitic acid (30 μM; Sigma Aldrich), oleic acid (30 μM; Sigma Aldrich), stearic acid (30 μM; Sigma Aldrich), and lipid mixture (2%; Sigma Aldrich). All fatty acids were conjugated with BSA. The cecal contents were lyophilized and the powder was dissolved in the advanced DMEM/F12 medium and added to organoids with titration.

Isolation of colonic mesenchymal stromal cells.

Colonic MSCs were isolated as described previously [40]. In brief, the remaining colon tissues after crypt isolation were added with DMEM medium (Gibco) containing 10% heat-inactivated FBS (Gibco), gentamycin /streptomycin, and collagenase type IV (Sigma Aldrich), and incubated for 1 hr at 37°C with shaking (200 rpm). Dissociated tissues were shaken vigorously and supernatants were passed through a 70 μm cell strainer (BD Falcon). Cell pellets were collected by centrifuge at 280 x g for 10 min, washed, and cultured with DMEM medium. MSCs were subcultured to obtain high purity cells. To test function of colonic MSCs from PD- and HFD-fed mice, MSCs (5×10^3 / well) were suspended in Matrigel in presence of organoids (1×10^4 / well) obtained from NCD-fed control mice or Apc^{Min}/J mice. After the Matrigel polymerized, ENR or WENR culture medium were added.

Flow cytometry.

Isolated colonic crypts and MSCs were analyzed by flow cytometry. For analysis of Lgr5-GFP^{+} cells, crypts were dissociated to individual cells with TrypLE Express (Thermo Fisher) at 37°C for 15 min and filtered out by a 40 μm cell strainer (BD Falcon). Dissociated crypt cells and MSCs were blocked with solution containing 0.2 % BSA in PBS and stained with Live/Dead cell stain kit (Thermo Fisher) and antibodies; anti-CD45 (clone 30-F11, BD Biosciences), anti-CD31 (clone MEC13.3, BD Biosciences), anti-PDGFR-α (clone EPR22059-270, abcam), and Alexa fluor 488-conjugated anti-rabbit IgG (Thermo Fisher). Flow cytometry was performed using a FACS CANTO II (BD Biosciences) and files were analyzed using FlowJo software (Tree Star).

Real time-qPCR.

RNA was extracted using the RNeasy mini kit (QIAGEN) from isolated colonic crypts. Thereafter, RNA was converted to cDNA with Superscript II reverse transcriptase and oligo (dT) primer (Thermo Fisher). cDNA was used as the template for real-time qPCR performed using SYBR green chemistry (Affymetrix) on an ABI 7500 Real Time qPCR system (Applied Biosystems). The primer sequences used for real-time qPCR are as follows: Lgr5, Fw 5'-CCTGTCCAGGCTTTCAGAAG-3', Rev 5'-CTGTGGAGTCCATCAAAGCA-3'; CD44, Fw 5'-TCCTTCTTTATCCGGAGCAC-3', Rev 5'-ACGTCTCCTGCTGGGTAGC-3'; Reg4, Fw 5'-CTGGAATCCCAGGACAAAGAGTG-3', Rev 5'-CTGGAGGCCTCCTC AATGTTTGC-3'; c-Kit, Fw 5'-TCATCGAGTGTGATGGGAAA-3', Rev 5'-GGTGACT TGTTTCAGGCACA-3'; EGF, Fw 5'-TTCTCACAAGGAAAGAGCATCTC-3', Rev 5'-GTCCTGTCCCGTTAAGGAAAAC-3'; EGFR, Fw 5'-GCTGGTGTTGCTGACCGCG-3', Rev 5'-GGGTGAGCCTGTTACTTGTGCC-3'; ErbB2, Fw 5'-GCAAGCACTGTCTGCCA TGC-3', Rev 5'-GGGCACAAGCCTCACACTGG-3'; Notch1, Fw 5'-GCTGCCTCTTTGA TGGCTTC-3', Rev 5'-CACATTCGGCACTGTTACAG-3'; DLL1, Fw 5'-CAGGACCTTC TTTCGCGTAT-3', Rev 5'-AAGGGGAATCGGATGGGGTT-3'; DLL4, Fw 5' TTCCAGG CAACCTTCTCCGA-3', Rev 5'-ACTGCCGCTATTCTTGTCCC-3'; Hes1, Fw 5'-CCAGC CAGTGTCAACACGA-3', Rev 5'-AATGCCGGGAGCTACTTTC-3'; FZD5, Fw 5'-CCGC ATACCACAAGCAAG-3', Rev 5'-GCATCAGCACCAAGAAGG-3'; CTNNB1, Fw 5'-AT GGAGCCGGACAGAAAAGC-3', Rev 5'-TGGGAGGTGTCAACATCTTC-3'; Axin2, Fw

5’-AACCTATGCCCGTTTCCTCT-3’, Rev 5’-GAGTGTAAAGACTTGG TCCA-3’; GSK3β, Fw 5’-ACCGACAACCACCTCCTTTG-3’, Rev 5’-TCACAGGGAGTGTCTGCTT G-3’; Cyclin D1, Fw 5’-GCGTACCCTGACACCAAT CTC- 3’, Rev 5’-CTCCTCTTCGCA CTTCTGCTC-3’; c-Myc, Fw 5’-TGAGCCCCTAGTGCTGCAT-3’, Rev 5’-AGCCCGAC TCCGACCTCTT-3’; LEF, Fw 5’-TGTTTATCCCATCA CGGGTGG-3’, Rev 5’-CATGGA AGTGTCGCCTGACAG-3’; APC, Fw 5’-AGCCATGC CAACAAAGTCATCACG-3’, Rev 5’-TTCCTTGCCACAGGTGGAGGTA-3’.

16s rRNA sequencing for metagenomic analysis.

Bacterial DNA was extracted from feces of mice fed PD and HFD using QIAamp DNA stool mini kits (Qiagen). PCR amplification was carried out using primers targeting the segment from V3 to V4 regions of the 16S rRNA gene with extracted DNA. For bacterial amplifications, we used barcoded primers of 341F (5′-CCTACGGGNBGCASCAG-3′) and 805R (5′-GACTACNVGGGTATCTAATCC-3′). The amplifications were performed by the following conditions: initial denaturation at 95 °C for 5 min, followed by 30 cycles of denaturation at 95 °C for 30 sec, primer annealing at 55 °C for 30 sec, and extension at 72 °C for 30 sec, with final elongation at 72 °C for 5 min. The QIAquick PCR purification kit (Qiagen) was used for the purification of the amplified products. Equal concentrations of purified products were pooled and short fragments (non-target products) were removed with an AMPure bead kit (Agencourt). The quality and product size were assessed on a Bioanalyzer 2100 (Agilent) using a DNA 7500 chip. Mixed amplicon sequencing was conducted by emulsion PCR and then deposited on picotiter plates. The sequencing was carried out at Chunlab (Seoul, South Korea) on a GS Junior Sequencing System (Roche), in accordance with the manufacturer’s instructions. Taxonomic cladogram was analyzed using LEfSe with a threshold 2 on the logarithmic LDA score [41].

Metabolomic analysis.

The cecal contents were lyophilized by Freeze Dryer (CHRIST) after pre-freezing overnight in -80°C. Cecal contents powder was homogenized well with cold methanol and internal standard solution (0.1 mg/mL myristic acid-d_{27}). Sample solutions were acidified with HCl

to 25 mM final concentration and centrifuged. Supernatants were collected into fresh tubes, and iso-octane was added. The upper phase was collected after liquid-liquid extraction process, and dried under vacuum. The dried sample was reacted with BCl_3-MeOH, 12 % w/w (Sigma-Aldrich) at 60 ℃ for 30min. H_2O and hexane were added sequentially and the sample was mixed vigorously. The upper phase was collected after resting the sample for 5 min. Then, anhydrous sodium sulfate was added and the supernatant was ready for GC/MS analysis. Fatty acid methyl esters (Sigma-Aldrich) were used to generate calibration curves without derivatization and analyzed with GC-MS system (Agilent7890A/5975C) using capillary column (HP-5MS, 30m × 0.25mm× 0.2μm). Electron impact (EI) ionization was used in positive ion mode. One μL of injection volume and split mode (ratio 10:1) were used. Extracted ion chromatogram by the specific fragment ion per fatty acid was used for quantification in the negative ion mode. Data analysis was performed using MSD Chemstation software (Agilent E02.02.1431).

Statistical analysis.

GraphPad Prism software (GraphPad) was used for statistical analysis. Significant differences between two groups were analyzed with two-tailed unpaired t-test. Multiple groups were analyzed by one- or two-way ANOVA followed by Bonferroni's post hoc test (*, $p < 0.05$; **, $p < 0.01$; ***, $p < 0.001$).

Result

HFD leads to pathological conditions in colon.

In order to confirm a role of HFD on the colon physiology, mice were fed PD or HFD for three month. Previous study clarified that there is significant differences between a refined diet and a chow diet in terms of gut microbiota composition and host physiology [42], we thus adopted PD as control diet of HFD. HFD contains 20% kcal carbohydrate, 60% kcal fat, and 20% kcal protein whereas PD contains 64% kcal carbohydrate, 16% kcal fat, and 20% kcal protein (Figure 3A). As expected, we observed higher body weight in mice fed HFD compared to those fed NCD or PD (Figure 3B). Unexpectedly, shorten colon length were found in both PD- and HFD-fed mice than those fed NCD (Figure 3C). We further addressed pathological changes of colon by HFD feeding in a steady-state condition. H&E staining indicated that histopathology score of colon was significantly higher in in HFD-fed mice than those in PD- or NCD-fed mice (Figure 4A). In addition, shorter crypt length and reduced goblet cells were found in HFD-fed mice (Figure 4B). Of note, significant alteration of colon pathology was also found in PD-fed mice, but less than HFD-fed mice (Figure 4A and 4B). Overall, we addressed that HFD induced significant pathological changes of colon in comparison to those of PD.

A

Ingredient	Purified diet g/kg
Casein	200
L-Cystine	3
Corn Starch	397.49
Maltodextrin 10	132
Sucrose	100
Solka Floc (Insoluble fiber)	50
Soybean Oil	70
Lard	0
Mineral & Vitamin	47.5
t-Butylhydroquinone	0.01
Total	1000

Ingredient	High fat diet g/kg
Casein	200
L-Cystine	3
Corn Starch	0
Maltodextrin 10	125
Sucrose	72.8
Solka Floc (Insoluble fiber)	50
Soybean Oil	25
Lard	245
Mineral & Vitamin	53
Dye	0.05
Total	773.85

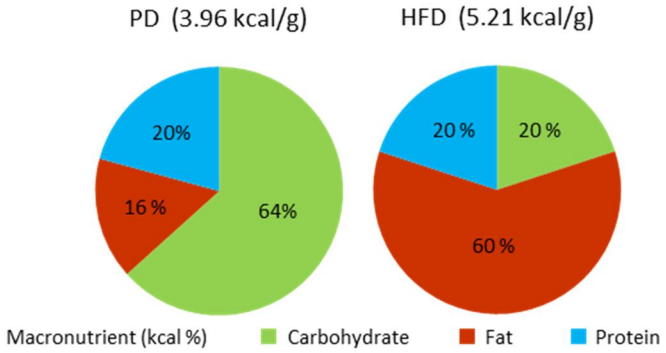

B

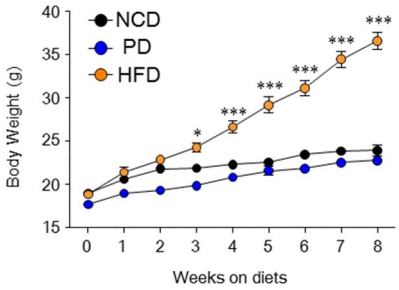

C

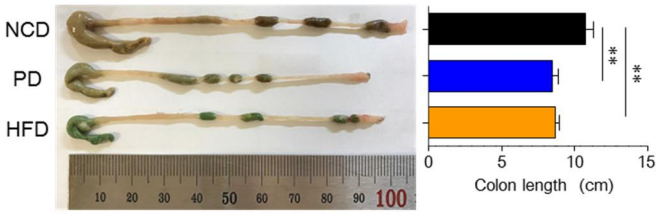

Figure 3. Alteration of body weight and colon length by HFD. Only HFD increased body weight whereas both purified diet (PD) or HFD feedings shortened colon length. (A) Macronutrient proportions and ingredients of PD or HFD. Changes of body weight for 2 months (B) and colon length (C) from mice fed PD or HFD for 4 months. n = 5 mouse / group. Data are mean ± s.e.m. Statistical analyses were done by Student's *t*-test. **p* < 0.05, ***p* < 0.01, ****p* < *0.001*.

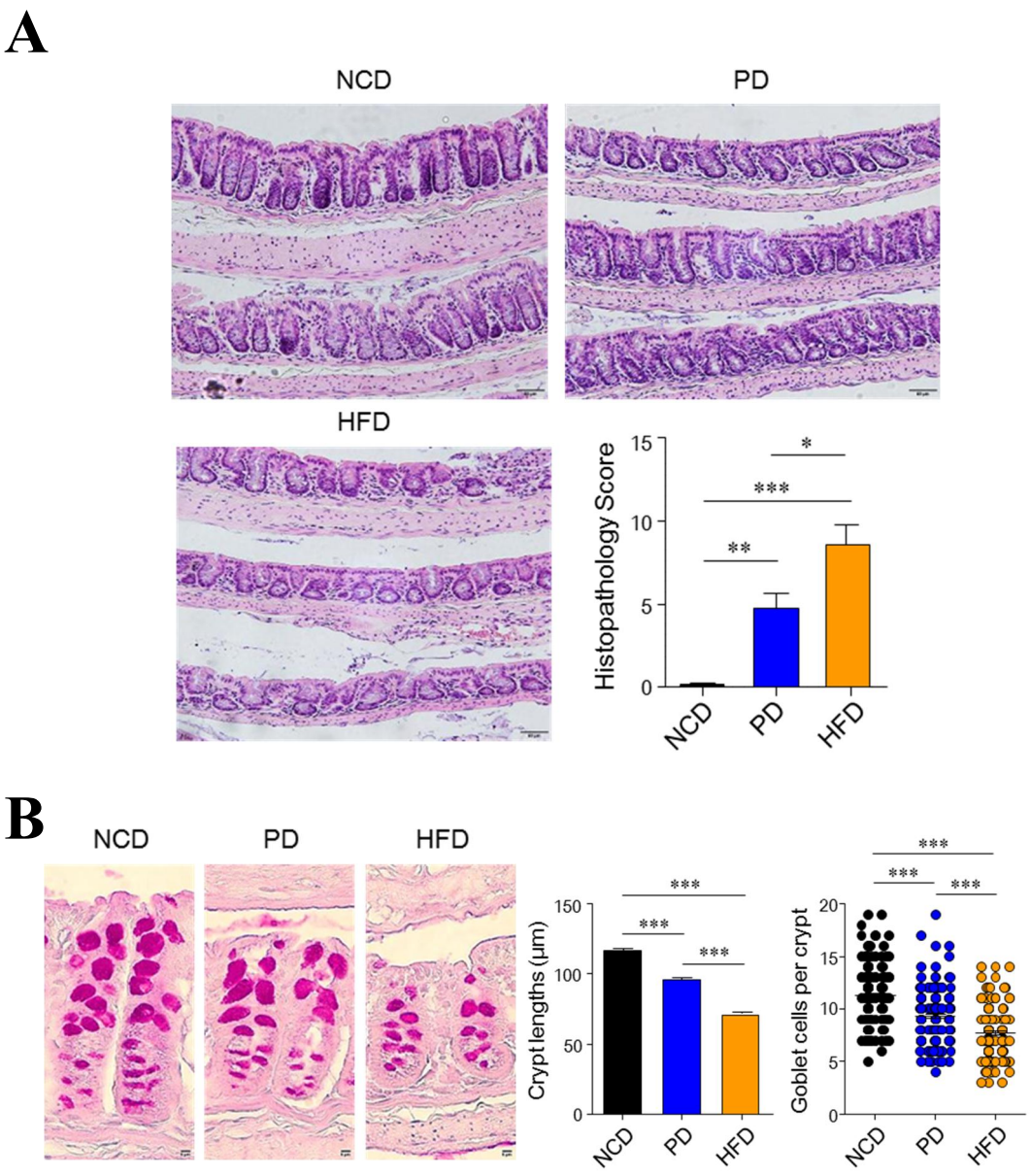

Figure 4. HFD resulted in pathological conditions in colon. Periodic acid-Schiff (PAS) and hematoxylin-eosin (H&E) staining of colon from mice fed HFD for 4 months. (A) Colon histology and histopathology score. Scale bar = 100 μm. (B) Representative images of colonic crypts from PAS staining, quantification of crypt length (n > 300 crypts), and goblet cell numbers (n > 100 crypts). Scale bar = 5 μm. Data are mean ± s.e.m. Statistical analyses were done by Student's *t*-test. *$p < 0.05$; **$p < 0.01$; ***$p < 0.001$.

HFD promotes the risk of colorectal cancer.

To confirm whether HFD control tumorigenesis as reported previously [30, 32], we administered AOM and DSS to groups of mice to induce inflammation-driven colorectal cancer (Figure 5A). As a result, almost HFD-fed mice were died within a few days after treatment with AOM (12.5 mg/kg body weight) whereas PD-fed mice died slowly (Figure 5B). Identical dose of AOM did not influence on the survival of NCD-fed mice. A survived HFD-fed mice (one from ten mice) possessed more polyps in the colon than those of mice fed NCD and PD (Figure 5D). As similar as the steady-state, colon length of mice fed PD or HFD were shorter than mice fed NCD (Figure 5C). These results indicate that HFD is more sensitive to AOM/DSS and promotes tumorigenesis in inflammation-derived colorectal cancer.

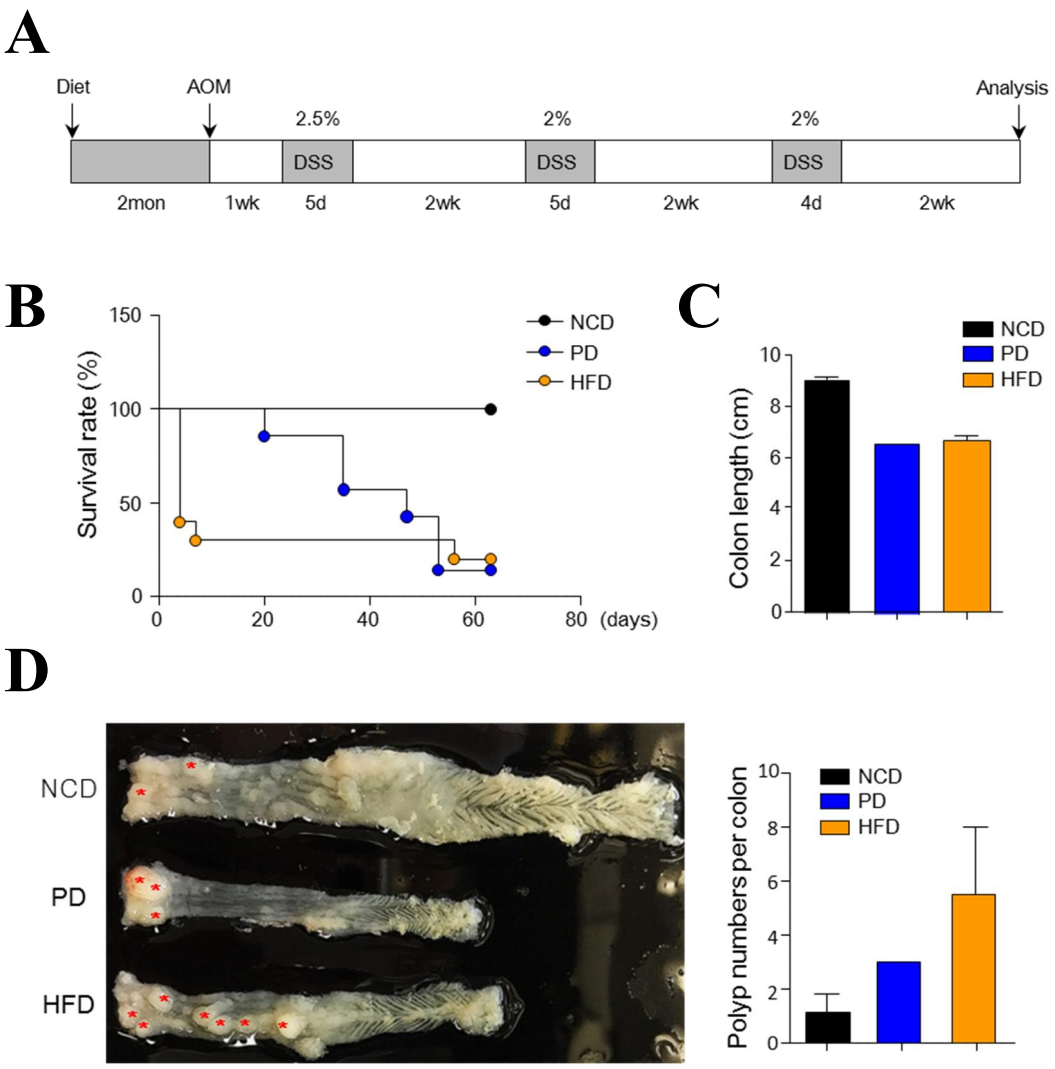

Figure 5. Increased incidence rate of colorectal cancer in HFD-fed mice. (A) Scheme for AOM/DSS colorectal cancer model. Survival rate (B) and colon length (C) of AOM/DSS-treated normal chow diet (NCD)-, purified diet (PD)-, and high fat diet (HFD)-fed mice. (D) Inflammation-induced colorectal cancer were induced by AOM plus DSS treatment. Polyp numbers per colon were counted. Red asterisks indicate polyps.

HFD enhances proliferation of ISC in colonic crypts.

We next analyzed the function of colon stem cells in relation to increased tumorigenesis from mice fed HFD. To assess how HFD affects ISCs and progenitors in colon, we used Lgr5-EGFP-IRES-CreERT2 mice. We first confirmed numbers of Lgr5-GFP^{+} cells in colon tissue of mice fed NCD or PD. Immunohistochemistry (IHC) approach revealed that numbers of Lgr5-GFP^{+} cells was increased in colonic crypts of mice fed HFD when compared to those of mice fed NCD but there was no significant difference between mice fed PD and HFD (Figure 6A). We further investigated Lgr5-GFP^{+} cells by distinguishing between GFP-expressing ISCs (Lgr5-GFP^{hi}) and progenitors (Lgr5-GFP^{low}) in the colon by FACS as reported previously [32]. Consistent with the IHC results, mice fed PD and HFD showed a tendency to increase frequency of Lgr5-GFP^{hi} ISCs in the colon but no difference in the frequency of Lgr5-GFP^{low} progenitors in comparison to mice fed NCD (Figure 6B). We next investigated the proliferation of colonic crypt cells by Ki67 staining in PD- or HFD-fed mice. Interestingly, Ki67-positive proliferating cells were more increased in proximal and distal colon region of HFD-fed mice than those of PD-fed mice, but no significant differences were found in the middle region of the colon (Figure 7). Importantly, Ki67-positive cells in the crypt bottom where ISCs exist significantly increased in HFD-fed mice than PD-fed mice. These results suggest that HFD promoted proliferating of ISCs in the colonic crypts.

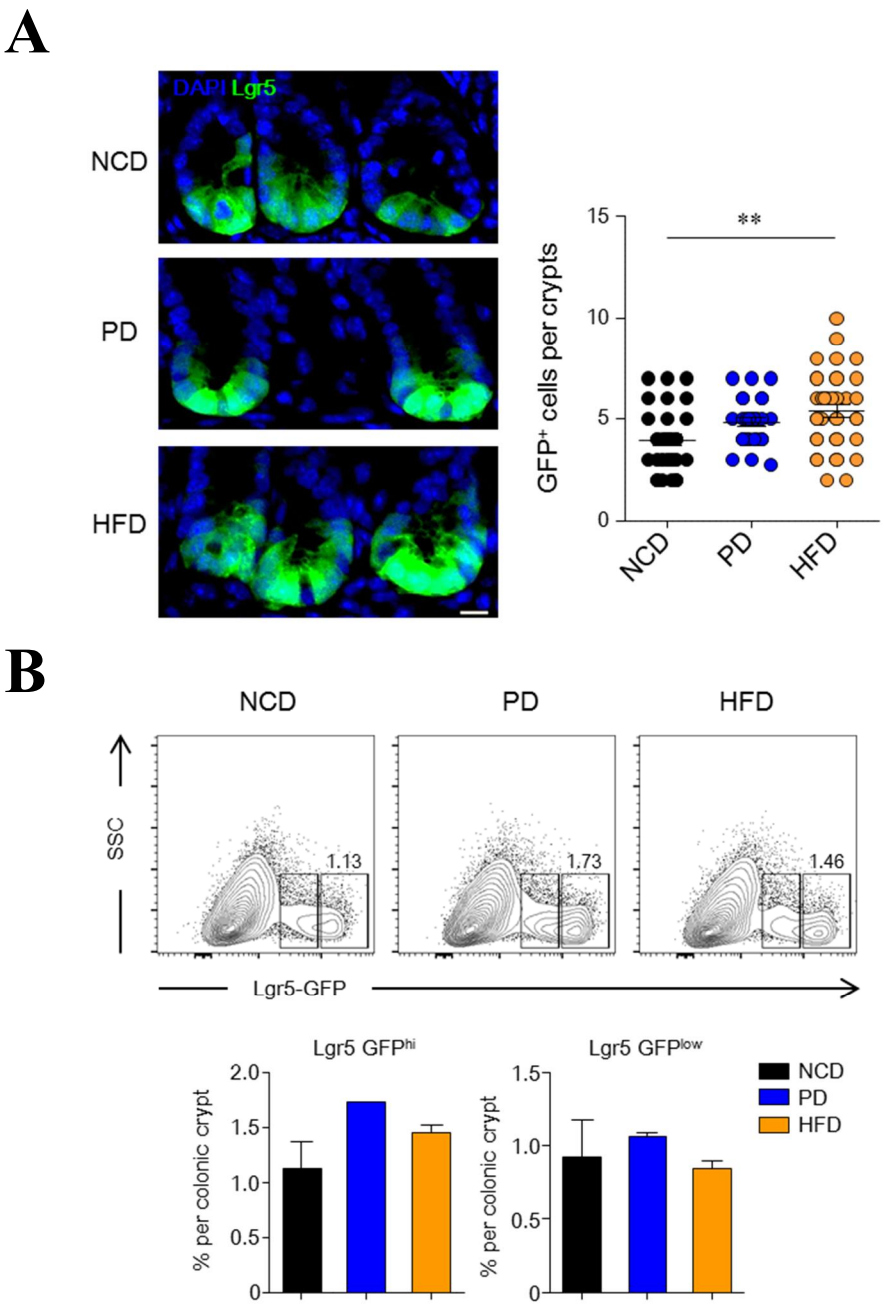

Figure 6. HFD modulated Lgr5^{+} intestinal stem cells (ISCs) in the colon. (A) Immunofluorescence image for Lgr5-expressed GFP^{+} cells in the colon tissues of PD- or HFD-fed mice. n = 3 mouse / group. Scale bar = 10 μm. (B) Percentage of ISCs (Lgr5-GFP^{hi}) and their progenitor cells (Lgr5-GFP^{low}) in the entire colonic crypt cells by flow cytometry analysis. Data are mean ± s.e.m. Statistical analyses were done by two-way ANOVA with Bonferroni *post-hoc* test. *$p < 0.01$; ***$p < 0.001$.

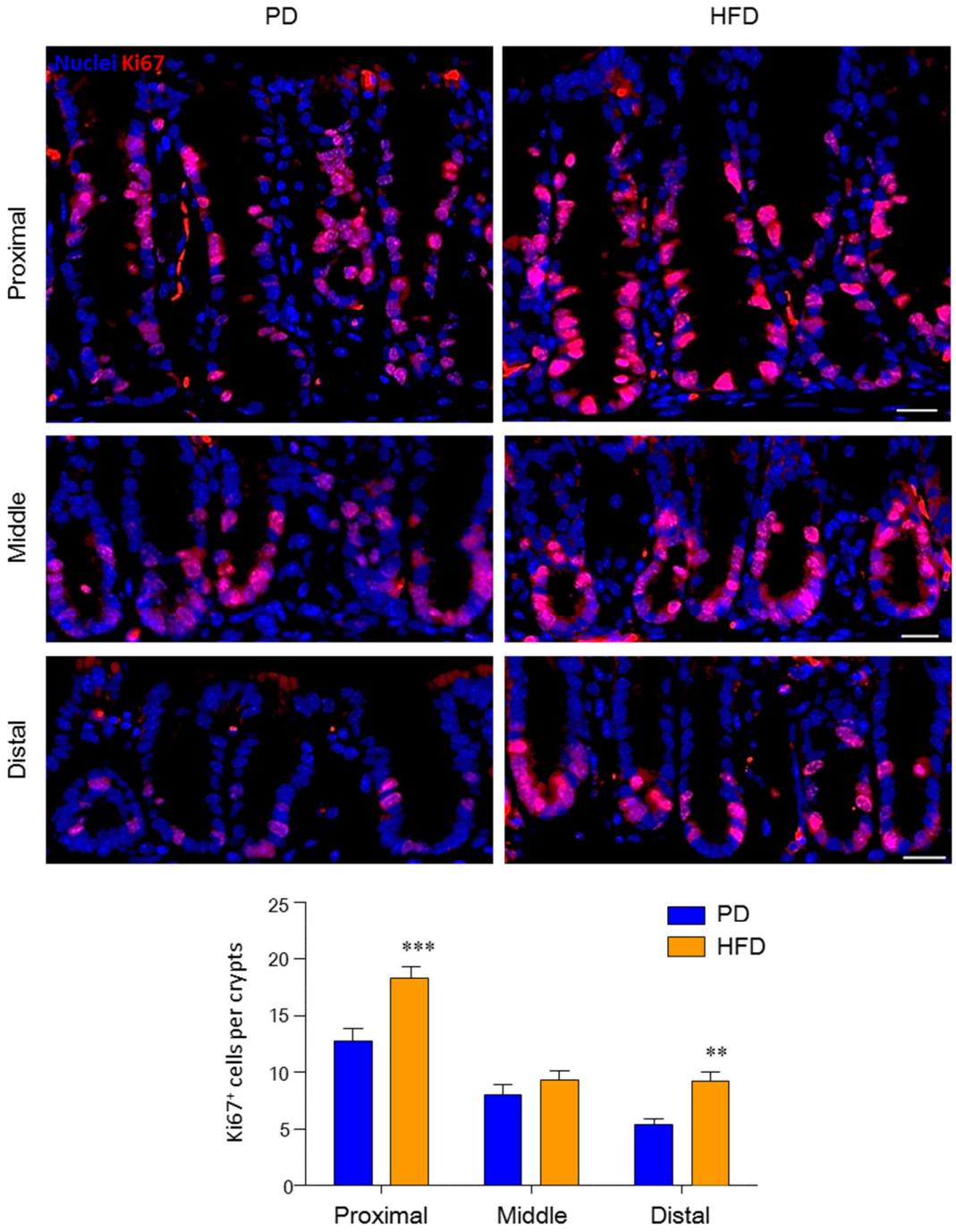

Figure 7. Proliferation of colonic epithelial cells was promoted by HFD. Immuno-fluorescence image for Ki67 expressions in the colon tissue of PD- or HFD-fed mice and quantification of $Ki67^+$ cells per crypt in proximal, middle, and distal regions of colon tissues. Scale bar = 20 μm. Data are mean ± s.e.m. Statistical analyses were done by two-way ANOVA with Bonferroni *post-hoc* test. $^{**}p < 0.01$, $^{***}p < 0.001$.

Hyper organogenesis of colonic crypts by HFD.

We next addressed if HFD also augments regeneration of colon tissue. Using an ex vivo 3-D culture system, we assessed the ability of isolated colonic crypts to form organoid bodies. Of interest, significantly enhanced organoid size in HFD-fed mice were addressed when compared to those in NCD- and PD-fed mice whereas no significant difference were found in organoid formation (Figure 8). These results support that HFD boosts the regenerative capacity of ISCs in the colon.

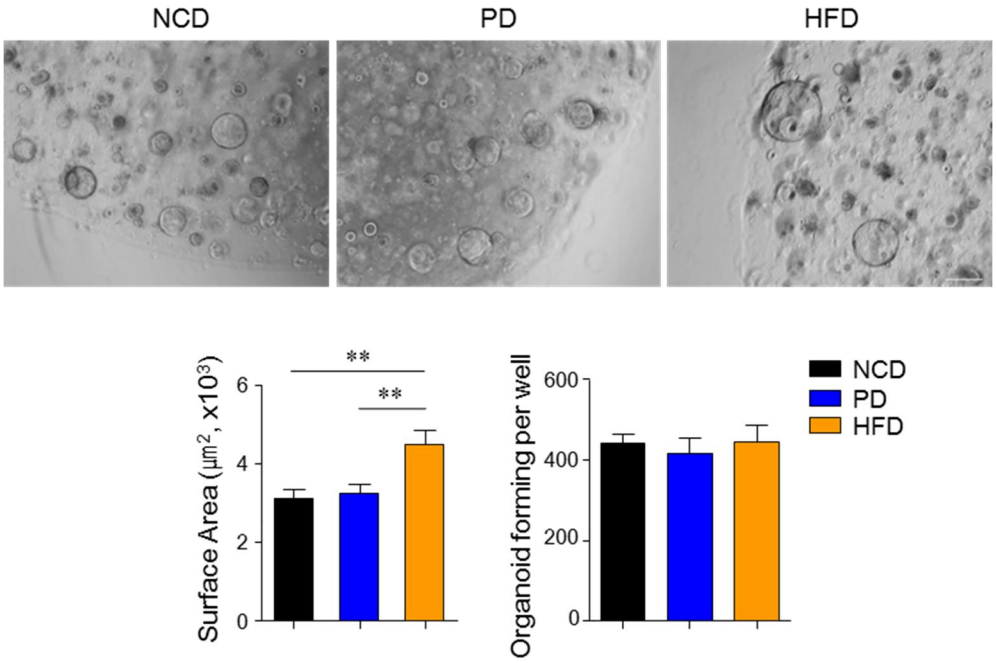

Figure 8. Overgrowth of colon organoids from HFD-fed mice. Colonic organoids were obtained from crypts of NCD-, PD-, and HFD-fed mice. Bright field images and quantification of colon organoids in the presence of WENR culture medium for 4 days. Surface area was measured at ≥50 organoids. Scale bar = 200 μm. Data are mean ± s.e.m. Statistical analyses were done by Student's *t*-test. $^{**}p < 0.01$.

HFD amplifies the Wnt signaling and CD44 expression in the colonic crypts.

To address factors regulating intestinal stemness in HFD-fed mice, we investigated mRNA expression level of genes associated with development of ISCs and DCS cells in colonic crypts using real-time qPCR. Of note, HFD amplifies gene expression of CD44 while no difference in the Lgr5 gene was found (Figure 9A). In contrast, gene expression of DCS cell markers such as Reg4 and c-Kit was reduced in the colonic crypts from HFD-fed mice when compared with those from PD-fed mice (Figure 9A). In addition, genes associated with EGF and Notch signaling was generally down regulated in mice fed HFD (Figure 9B). In order to clarify EGF- and Notch-independent pathway, we further analyzed genes related to Wnt/β-catenin pathway. Among Wnt/β-catenin-related genes, Axin2, Cyclin D1 and APC were significantly increased in HFD-fed mice when compared with those from PD-fed mice (Figure 10A). The mRNA levels of Axin2 expression was also confirmed by *in situ* hybridization (Figure 10B). We also observed significantly higher nuclear β-catenin accumulation in the colon tissue of mice fed HFD than those of PD-fed mice (Figure 11). These data support the notion that HFD amplifies CD44 expression associated with ISC activity and up-regulates Wnt/β-catenin signaling in the colon.

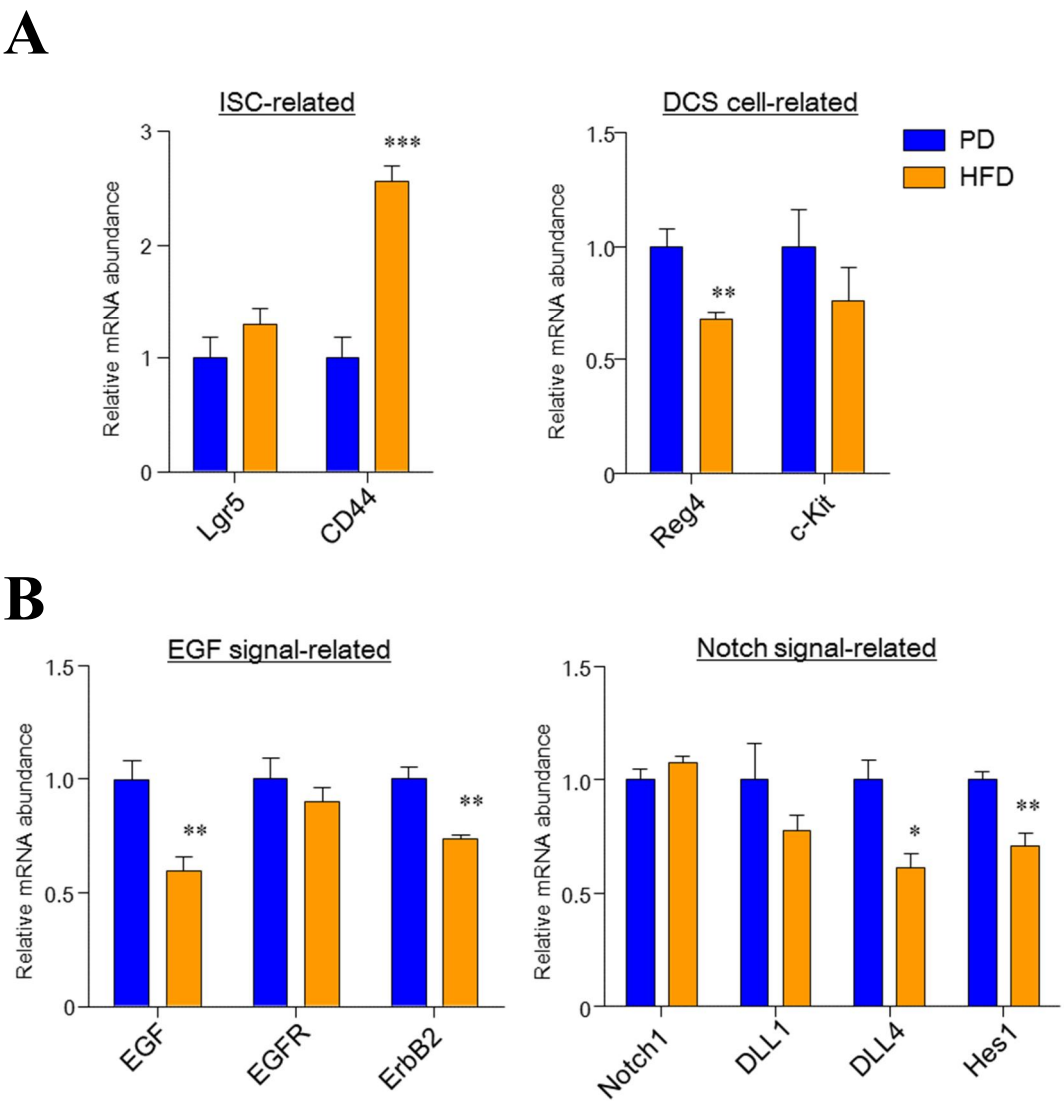

Figure 9. HFD increased CD44 expression associated with ISCs in the colon. (A) Relative mRNA expression level of genes associated with ISCs and deep crypt secretory (DCS) cells. (B) Gene expression levels related with EGF and Notch signal pathways were measured by real-time PCR in the colonic crypts. Expression shown is relative to β-actin gene. n = 3 mouse / group. Data are mean ± s.e.m. Statistical analyses were done by Student's *t*-test. **p* < 0.05; ***p* < 0.01; ****p* < *0.001*.

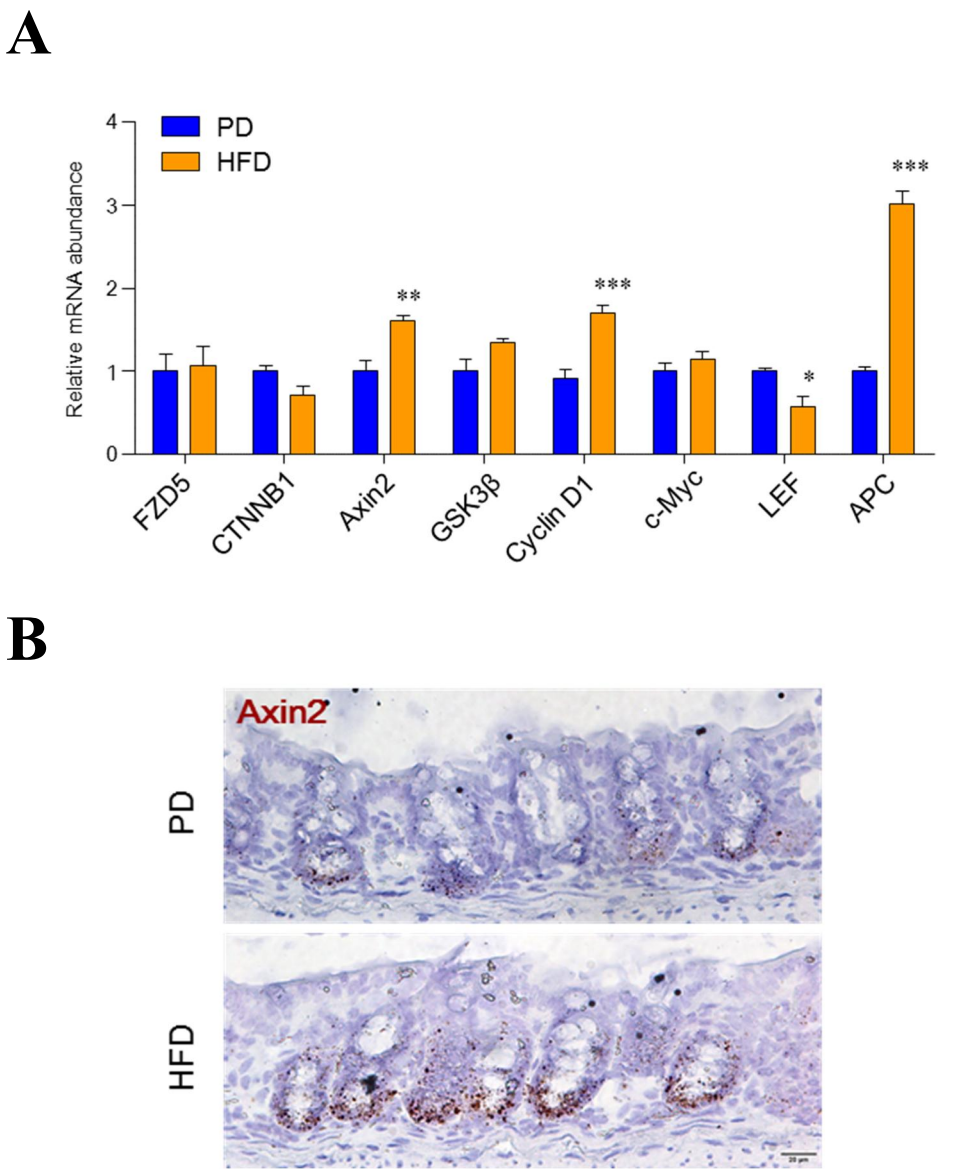

Figure 10. HFD augments Wnt signaling in the colon epithelial crypts. (A) Relative mRNA expression level of genes associated with Wnt signaling was measured in the colonic crypts by real-time PCR. (B) *in situ* hybridizations of *Axin2* expression in the colon obtained from PD- or HFD- fed mice. n ≥ 2. Data are mean ± s.e.m. Statistical analyses were done by Student's *t*-test. Scale bar = 20 μm. *$p < 0.05$; **$p < 0.01$; ***$p < 0.001$.

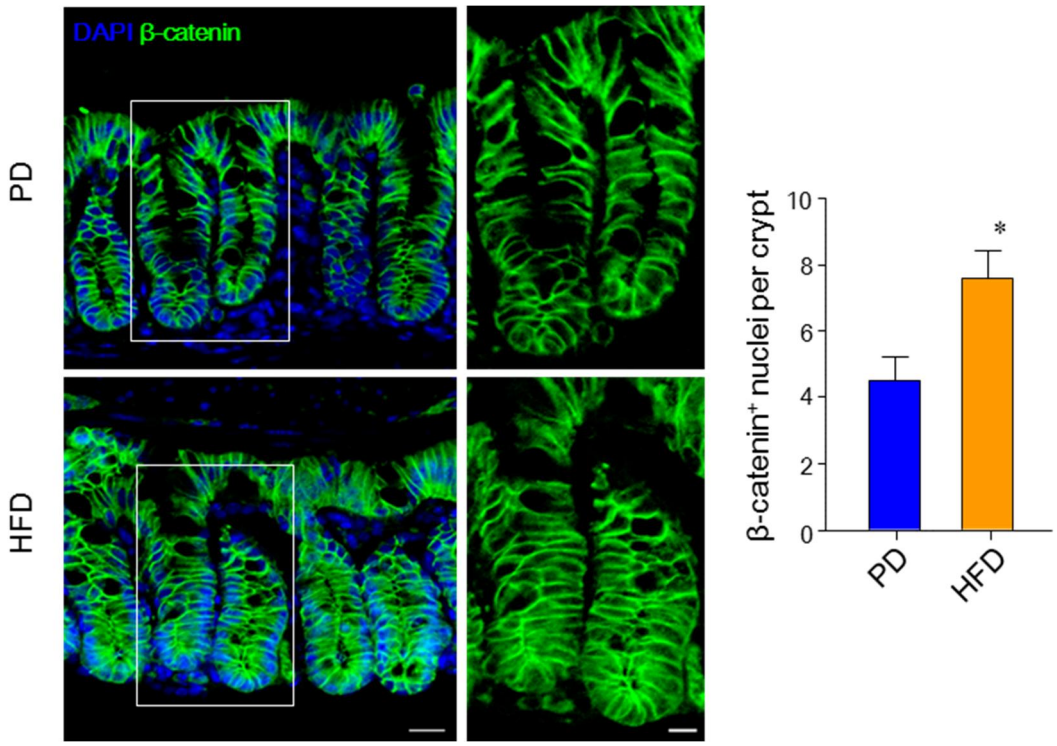

Figure 11. HFD increased β-catenin translocation into the nucleus in the colonic crypts. Immunofluorescence image of nuclei (blue) and β-catenin (green) and quantification of nuclear β-catenin localization from confocal image in colonic crypts obtained from PD- or HFD- fed mice. Scale bar = 20 μm (left panel) and 5 μm (right panel). Data are mean ± s.e.m. Statistical analyses were done by Student's *t*-test. *$p < 0.05$.

HFD stimulates Wnt2b secretion from PDGFR-α^{+} MSCs.

Unlike the Paneth cells in the small intestine, colonic DCS cells are not known to secrete Wnt ligands [11]. Accordingly, we hypothesized that MSCs might be another candidate to control Wnt/β-catenin signaling in the colon under HFD condition. Wnt2b expression, one of the major Wnt liands secreted by colonic MSCs, was significantly increased in subepithelium and submucosa regions of colon from mice fed HFD when compared with those from mice fed PD (Figure 12A). Then, colonic MSCs were isolated from each group of mice and Wnt2b expression levels were addressed. As shown in Figure 12B, Wnt2b expressions were considerably higher in αSMA^{+} MSCs isolated from HFD-fed mice than (Figure 12D). We next investigated whether HFD-derived MSCs promote colon organoid growth and formation in ENR and WENR medium condition. In the presence of WENR medium, the size of organoids co-cultured with HFD-derived MSCs was more enhanced than those with PD-derived MSC, but there was no difference in organoid formation (Figure 13A). In the presence of ENR medium, HFD-derived MSCs promoted both size and formation of organoids than PD-derived MSCs (Figure 13B). Furthermore, co-cultured with HFD-derived MSCs promoted the size and formation of colon cancer organoids derived from $Apc^{Min/+}$ mice when compared with PD-derived MSCs (Figure 13C). These data indicates that HFD promotes proliferation of ISCs and CSCs through stimulation of Wnt2b in PDGFR-α^{+} MSCs.

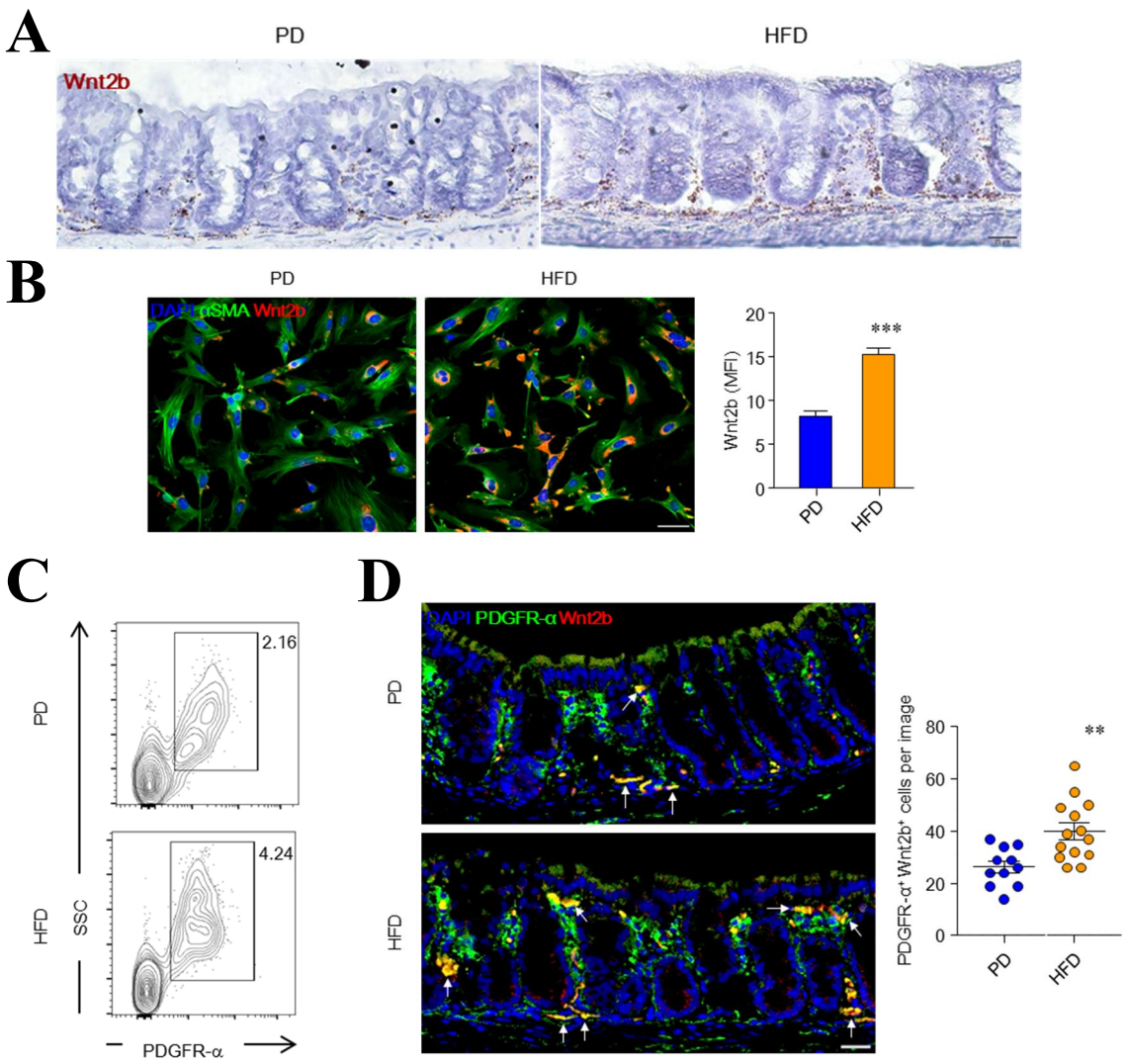

Figure 12. Wnt2b secretion was promoted by PDGFR-a$^+$ MSCs in the colon following HFD. (A) Representative *in situ* hybridizations images of Wnt2b in the colon tissues from PD- or HFD-fed mice. (B) Immunofluorescence image of Nuclei (blue), αSMA (green), and Wnt2b (red) in the colonic MSCs isolated from PD- or HFD-fed mice. Quantification for Wnt2b was measured at ≥ 90 cells by mean fluorescence intensity (MFI). (C) Populations of PDGFR-α$^+$ MSCs in the colon were measured by flow cytometry. (D) Immunofluorescence image of Nuclei (blue), PDGFR-α (green), and Wnt2b (red) in colon from PD- or HFD-fed mice and quantification for PDGFR-α$^+$Wnt2b$^+$ cell were measured by ImageJ (n=3). White arrows indicate PDGFR-α$^+$Wnt2b$^+$ cells. Scale bar = 20 μm (A, D), 50 μm (B). Data are mean ± s.e.m. Statistical analyses were done by Student's *t*-test. $^{**}p < 0.01$; $^{***}p < 0.001$.

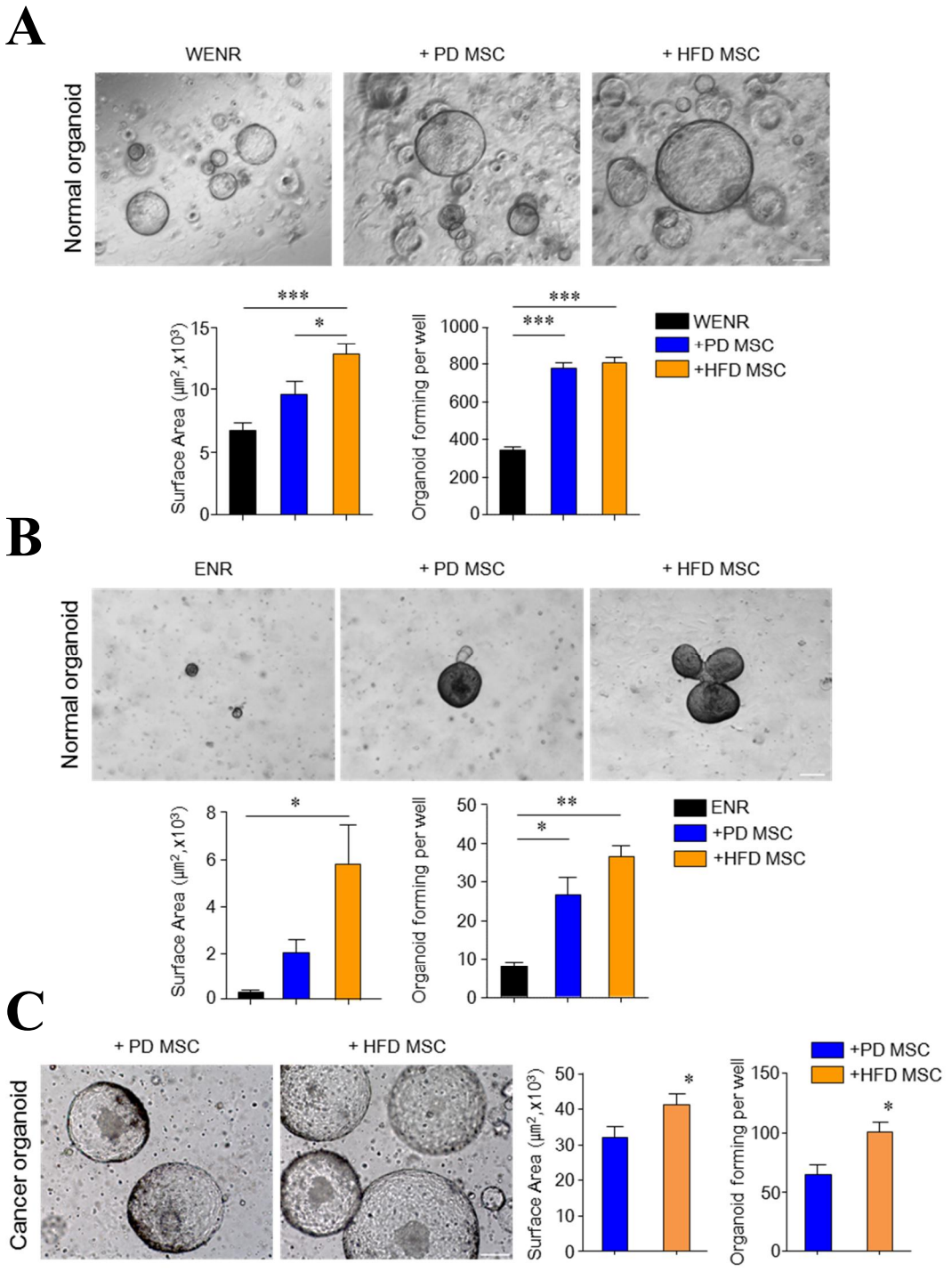
A
WENR
+ PD MSC
+ HFD MSC
Normal organoid
Surface Area (μm², x10³)
Organoid forming per well
WENR
+PD MSC
+HFD MSC
B
ENR
+ PD MSC
+ HFD MSC
Normal organoid
Surface Area (μm², x10³)
Organoid forming per well
ENR
+PD MSC
+HFD MSC
C
+ PD MSC
+ HFD MSC
Cancer organoid
Surface Area (μm², x10³)
Organoid forming per well
+PD MSC
+HFD MSC

Figure 13. Colonic MSCs isolated from HFD-fed mice enhance organoid growth. Colon organoids from mice were co-cultured with MSCs from PD- or HFD-fed mice. (A) Colon organoids were co-cultured in the presence of WENR medium and quantification (surface area and organoid-forming numbers) were measured on day 7 (n > 60). (B) Colon organoids co-cultured in the presence of ENR medium and quantification were measured on day 4 (n > 60). (C) Colon cancer organoids obtained from $Apc^{min/+}$ mice were co-cultured with MSCs from PD- or HFD-fed mice in the presence of EN medium and quantification were measured on day 6 (n > 50). Scale bar = 200 μm. Data are mean ± s.e.m. Statistical analyses were done by two-way ANOVA with Bonferroni *post-hoc* test. **p* < 0.05; ***p* < 0.01; ****p* < *0.001*.

B

a

c

t

e

r

o

i

d

e

t

Principal component analysis (PCA) of unweighted UniFrac and weighted UniFrac revealed an evident separation of gut microbiota composition between PD- and HFD-fed mice (Figure 14B). In addition, the results of the Shannon index, Chao1, and operational taxonomic units (OTUs) indicated that the diversity of resident gut microbiota in HFD-fed mice was decreased when compared with those in PD-fed one (Figure 14C). We hypothesized that gut microbiota-derived metabolites may affect ISC niche.

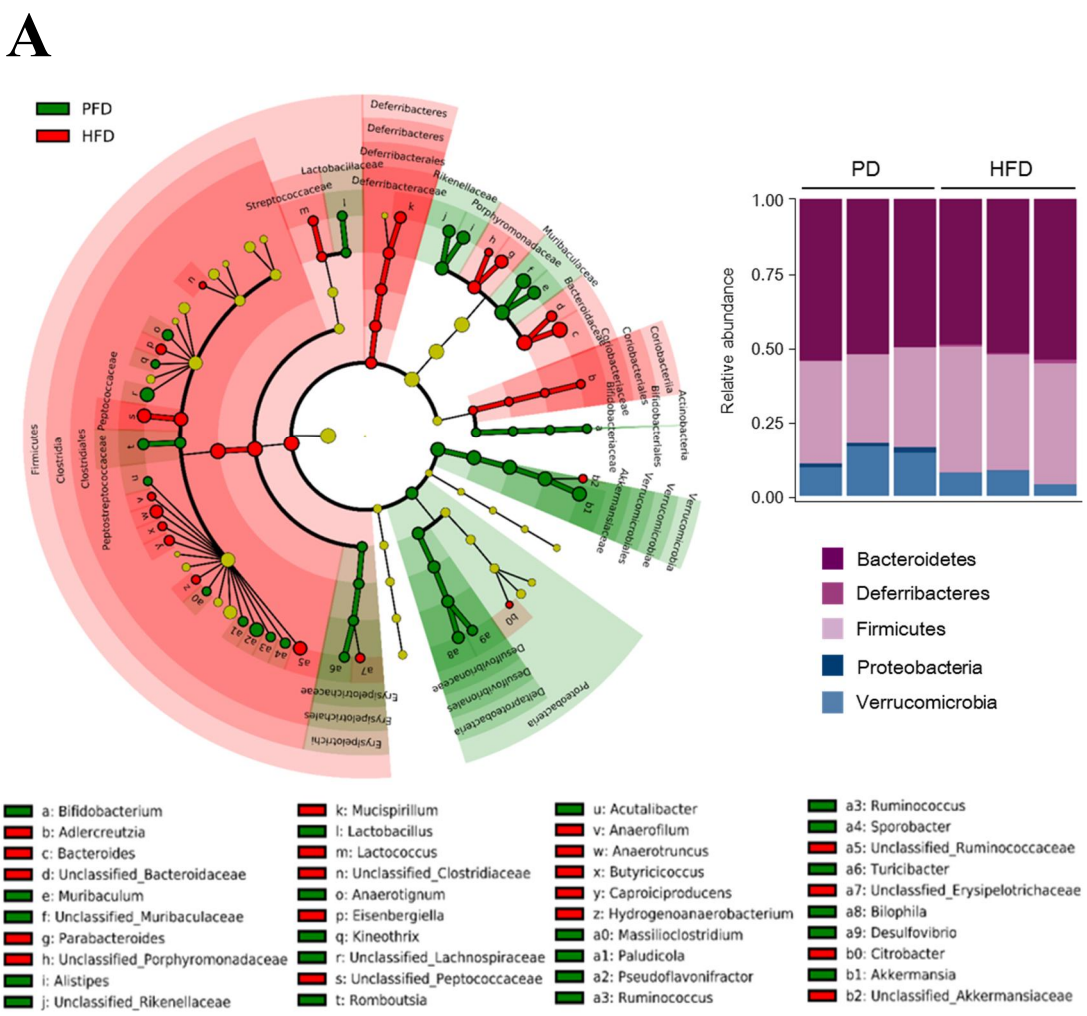
A
PFD
HFD
PD
HFD
Relative abundance
1.00
0.75
0.50
0.25
0.00
Bacteroidetes
Deferribacteres
Firmicutes
Proteobacteria
Verrucomicrobia
a: Bifidobacterium
b: Adlercreutzia
c: Bacteroides
d: Unclassified_Bacteroidaceae
e: Muribaculum
f: Unclassified_Muribaculaceae
g: Parabacteroides
h: Unclassified_Porphyromonadaceae
i: Alistipes
j: Unclassified_Rikenellaceae
k: Mucispirillum
l: Lactobacillus
m: Lactococcus
n: Unclassified_Clostridiaceae
o: Anaerotignum
p: Eisenbergiella
q: Kineothrix
r: Unclassified_Lachnospiraceae
s: Unclassified_Peptococcaceae
t: Romboutsia
u: Acutalibacter
v: Anaerofilum
w: Anaerotruncus
x: Butyricicoccus
y: Caproiciproducens
z: Hydrogenoanaerobacterium
a0: Massilioclostridium
a1: Paludicola
a2: Pseudoflavonifractor
a3: Ruminococcus
a3: Ruminococcus
a4: Sporobacter
a5: Unclassified_Ruminococcaceae
a6: Turicibacter
a7: Unclassfied_Erysipelotrichaceae
a8: Bilophila
a9: Desulfovibrio
b0: Citrobacter
b1: Akkermansia
b2: Unclassified_Akkermansiaceae

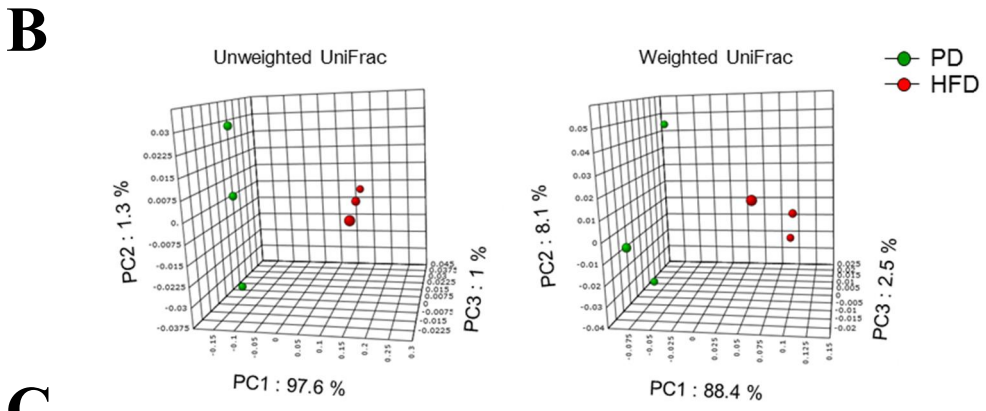
B
Unweighted UniFrac
Weighted UniFrac
PD
HFD
PC2 : 1.3 %
PC3 : 1 %
PC1 : 97.6 %
PC2 : 8.1 %
PC3 : 2.5 %
PC1 : 88.4 %

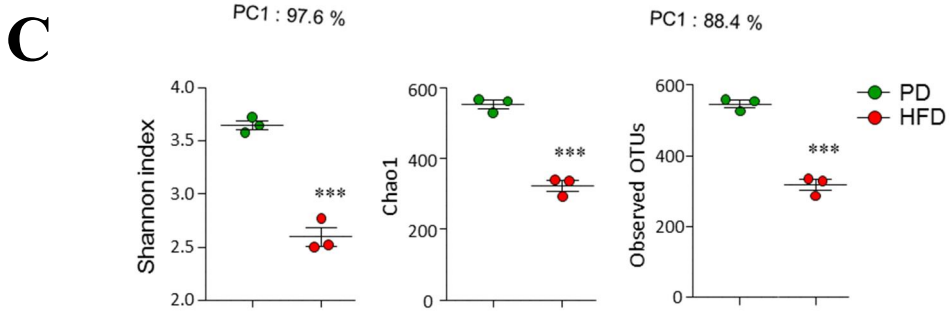
C
Shannon index
Chao1
Observed OTUs
***
***
***
PD
HFD

Figure 14. Differences at genus levels of gut microbiota were determined by linear discriminant analysis using LEfSe. Pyrosequencing analysis for gut microbiota was determined from feces of PD- or HFD-fed mice. (A) Microbiome composition (left panel) and relative abundance (right panel) in the feces from PD- or HFD-fed mice for 3 months. n = 3 mouse / group. (B) Principal component analysis (PCA) of unweighted UniFrac and weighted UniFrac distances was analyzed for clustering fecal microbial communities between two groups. (C) Shannon index, Chao1, and OTUs of gut microbiota were determined. Data are mean ± s.e.m. Statistical analyses were done by Student's *t*-test. ***$p < 0.001$.

Increased FFA by HFD promotes colon organogenesis.

To address a role of gut metabolites on the pathophysiological role of HFD, we treated cecal contents of PD- or HFD-fed mice to colon organoids obtained from naïve B6 mice. As a result, cecal contents derived from HFD-fed mice stimulated organoid growth more than those from PD-fed mice (Figure 15A). To determine which components in the cecal contents of HFD-fed mice promote organogenesis, we analyzed short chain fatty acid (SCFA) in cecal contents of mice fed PD or HFD. Unexpectedly, there was no difference when SCFA level was compared in cecal contents of mice fed PD or HFD (data not shown). We thus investigated whether FFA by HFD induces dysfunction in ISCs and their niche. First, we analyzed FFA level in cecal contents of mice fed PD or HFD, and found that FFA levels were significantly increased in HFD-fed mice when compared with those from PD-fed mice (Figure 15B). We next selected palmitic acid (PA), stearic acid (SA), oleic acid (OA), and the lipid mixture (LM), and added them to the colon organoids of naive mice in the presence of WENR medium to assess the ability of FFA to promote organogenesis. All selected FFAs and LM increased the size of organoids significantly (Figure 15C). These results indicate that FFA increased by HFD promoted ISC function in the colon.

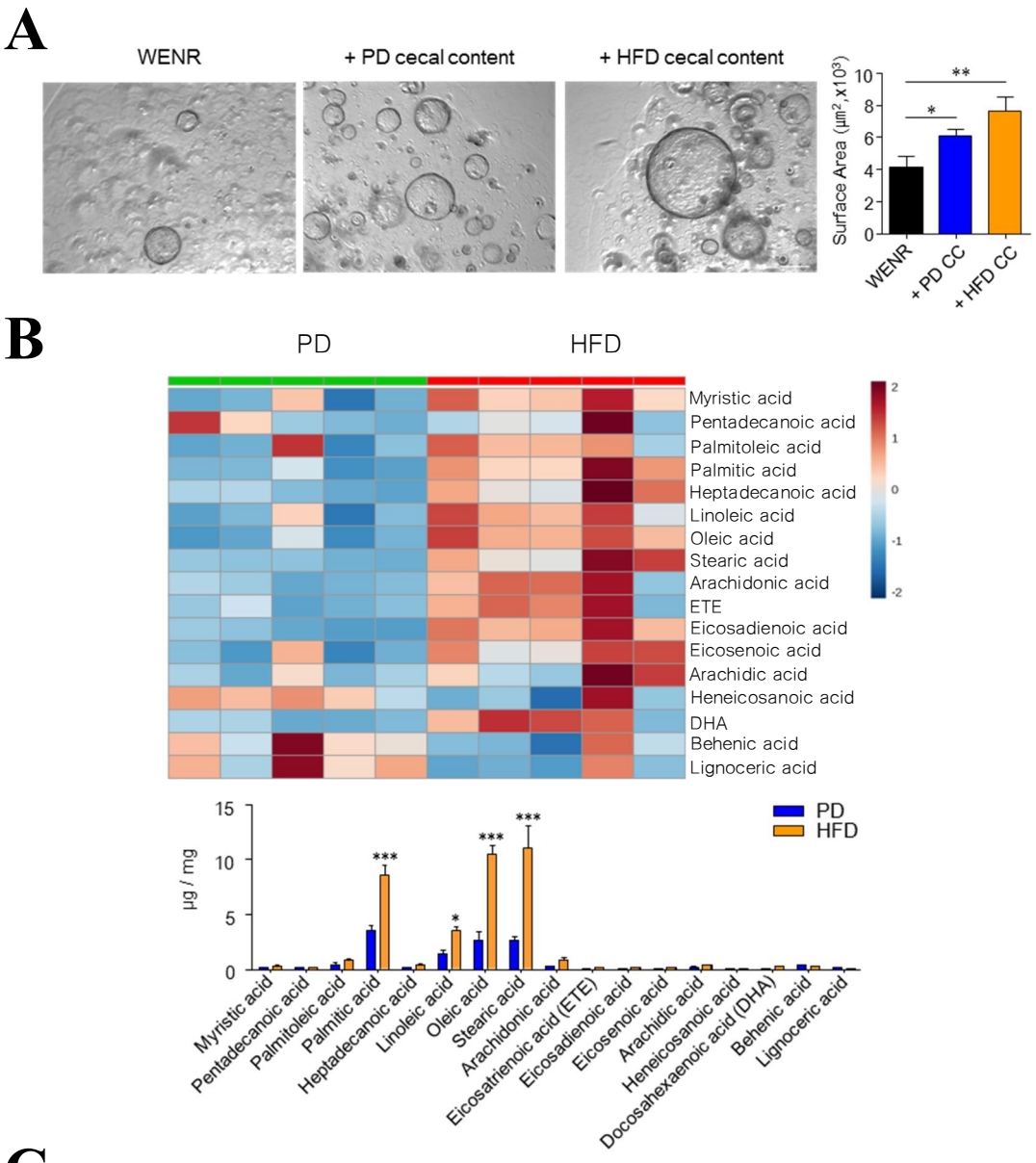
A
WENR
+ PD cecal content
+ HFD cecal content
Surface Area (μm², x10³)
WENR
+ PD CC
+ HFD CC
B
PD
HFD
Myristic acid
Pentadecanoic acid
Palmitoleic acid
Palmitic acid
Heptadecanoic acid
Linoleic acid
Oleic acid
Stearic acid
Arachidonic acid
ETE
Eicosadienoic acid
Eicosenoic acid
Arachidic acid
Heneicosanoic acid
DHA
Behenic acid
Lignoceric acid
μg / mg
PD
HFD
Eicosatrienoic acid (ETE)
Docosahexaenoic acid (DHA)
C
ENR
PA
SA
OA
LM
Surface Area (μm², x10³)

Figure 15. Free-fatty-acids in the cecal contents of HFD promotes gut organogenesis. (A) Colon organoids of naïve B6 mice were co-cultured with cecal contents from PD- or HFD-fed mice for 4 days. Surface area was measured at 30 ≥ organoids. (B) Level of free-fatty-acids (FFA) was analyzed in the cecal contents of PD- and HFD-fed B6 mice for 5 months. (C) Colon organoids of naïve B6 mice were cultured with Palmitic acid (PA), Stearic acid (SA), Oleic acid (OA), or Lipid mixture (LM) for 4 days. Surface area was measured at ≥ 40 organoids. Data are mean ± s.e.m. Statistical analyses were done by Student's *t*-test. Scale bar = 50 μm (C), 200 μm (B). *$p < 0.05$; **$p < 0.01$; ***$p < 0.001$.

Discussion

Although dietary signals are known to be important for ISC and Paneth cell biology, the role of dietary signals in intestinal MSCs are not well known. In this study, we demonstrate that dysregulation of MSCs and increased incidence rate of colorectal cancer in HFD-fed mice through in vivo mouse model and ex vivo organoid studies. HFD feeding promoted expression of CD44, one of cancer stem cell markers, in ISC and Wnt-related signals in the colonic crypts. Especially, numbers and Wnt2b expression of PDGFR-α^+ MSCs in the colon were significantly enhanced by HFD feeding. Co-cultured with HFD-derived MSCs resulted in hyper organogenesis of normal and cancer stem cells. These results imply that colon PDGFR-α^+ MSCs play indispensable role on control of cancer stem cells in HFD-induced obesity.

We found that pathological conditions such as reduction of crypt length and goblet cell numbers, and low grade inflammation were significantly induced in the colon of HFD-fed mice when compared with those of NCD- or PD-fed mice (Figure 3). The fact that mild changes of pathological conditions in the colon were also found in PD-fed mice, indicating that choosing appropriated control diet might be crucial factor for HFD study. In this regards, Dalby et al. revealed that effectiveness of HFD in gut microbiota composition due to diet type, not obesity itself [42].

Obese microbiota is known to induce pathophysiology of obesity by increasing energy harvesting ability [44, 45]. Indeed, completely separated composition and reduced diversity of gut microbiota were identified in HFD-fed mice when compared to PD-fed mice (Figure 14). Previous studies have suggested an increase in Firmicutes-to-Bacteroidetes ratio as characteristics of obese microbiota [44, 45]. In our study, the abundance of Bacteroidetes did not differ, but the abundance of Firmicutes significantly increased in HFD condition. On the other hands, Lee et al. identified that HFD-fed mice were more susceptible to DSS-induced colitis, accompany by the expansion of selected pathobionts such as *Atopobium* spp. and Proteobacteria [46]. Instead of expansion of selected pathobionts, we found here that the abundance of Verrucomicrobia, to which the *Akkermensia* genus belongs, is reduced in HFD

condition. *Akkermansia muciniphila* has been shown to have a role in energy homeostasis, glucose metabolism, and gut barrier function [47, 48]. Therefore, HFD-induced dysbiosis such as decreasing *A.muciniphila* might be associated with obesity-related pathophysiology.

Recent studies have reported that dietary signals regulate ISCs and their niche in the intestinal epithelium [29-31]. We confirmed that HFD enhances proliferation of ISCs in colonic crypts as reported previously [32]. Of note, we identified that CD44 expression was significantly increased in the colonic crypts of HFD-fed mice while EGF signal- and Notch signal-related genes were mostly down-regulated (Figure 9). CD44 is known as Wnt signaling target genes [49, 50]. Consistent with the increase in CD44, HFD increased gene expression associated with Wnt signaling in the colonic crypts. Importantly, CD44 has been reported to be overexpressed in colorectal cancer and considered as a signature marker for CSCs, which are known to be responsible for the initiation of cancer [51, 52]. Furthermore, CD44 has been reported to modulate epithelial-mesenchymal transitions which associated with metastatic potential [53]. Taken together, increased expression of CD44 in the colonic crypts might be crucially associated with tumorigenesis in HFD [23].

Overexpression of Wnt ligands is well known to be associated with tumors [28, 54, 55]. We aimed to identify fundamental cells which boost Wnt ligands in the colonic crypts under HFD condition. Of note, HFD promoted numbers and Wnt2b secretion of PDGFR-α^+ MSCs in the colon (Figure 12). These results were supported by the fact that HFD-derived MSCs promote more organogenesis than PD-derived one (Figure 13). Previous studies have shown that obesity increases differentiation of adipose-derived MSCs into myofibroblasts and production of ECM components, which promote breast tumorigenesis [56]. As tumor microenvironment, cancer-associated fibroblasts (CAF) have been found in various cancers and the plentiful of those cells in tumor is associated with poor prognosis in patients, and they provide evidence of functional significance and prognostic value [57, 58]. It has been reported that CAF contains a paracrine communication in tumor microenvironment, which promotes tumor progression and metastasis [59-61]. Likewise, our study demonstrated that Wnt2b overexpression from colon PDGFR-α^+ MSCs was found in HFD condition and that it promoted organogenesis. Moreover, PDGFR-α is known as a marker of normal intestinal

MSCs but paradoxically reported as a CAF marker [22, 62, 63]. We thus speculate that PDGFR-α^+ MSCs in the colon that overexpressed Wnt2b by HFD may be substantial source for increased tumorigenesis.

We found that cecal contents obtained from mice fed HFD promote organogenesis when compared with those from mice fed PD. Among the metabolites in the cecal contents, FFA levels were predominantly increased by HFD (Figure 15). FFA has been reported to activate ISC function such as self-renewal and proliferation directly through PPAR-δ signaling activation by FFA. [32]. We identified that direct effect of FFA on ISCs, and as a result, FFA such as PA, SA, OA and LM enhanced organogenesis of colonic crypts. Consistently, others found that PPAR-δ signaling activation by FFA enhances ISC function through fatty acid oxidation [64]. Therefore, the ISC function can be directly affected by the increased FFA under the HFD condition.

Overall, our study demonstrated that predominant expression of CD44 on colonic crypts was induced by HFD. In metabolomics and organoid analysis, we identified that HFD-induced FFA resulted in the self-renewal of ISCs directly. Moreover, the function of normal and malignant ISCs was further stimulated as a non-autonomous effect in the presence of PDGFR-α^+ MSCs. Hence, these finding implies that PDGFR-α^+ MSCs and FFA may be considered as clinical targets for colorectal cancer in obesity.

Conclusion

HFD feeding increased tumorigenesis in AOM/DSS mice model and stimulated proliferation of colonic crypt cells in the steady-state condition. We demonstrated that reduced expression of genes associated with DCS cells as well as the number of goblet cells in the colonic crypts. Instead, HFD activated Wnt signaling of ISCs in the colonic stem cells, which was triggered by the Wnt2b overexpression from the PDGFR-α^+ MSCs. We showed through organogenesis analysis that MSCs dysregulation by HFD feeding can further promote self-renewal of normal and malignant CSCs. In addition, a significant increase in CD44 expression, known as the CSC marker, was found in the colonic crypt of mice fed HFD. Of note, HFD feeding directly increased the self-renewal of ISCs through increased FFA. These results imply that FFA and dysregulation of PDGFR-α^+ MSC may contribute to colorectal cancer development in HFD condition. Furthermore, CD44 overexpression in HFD-fed mice may be a clue to transformation from normal stem cell to CSCs.

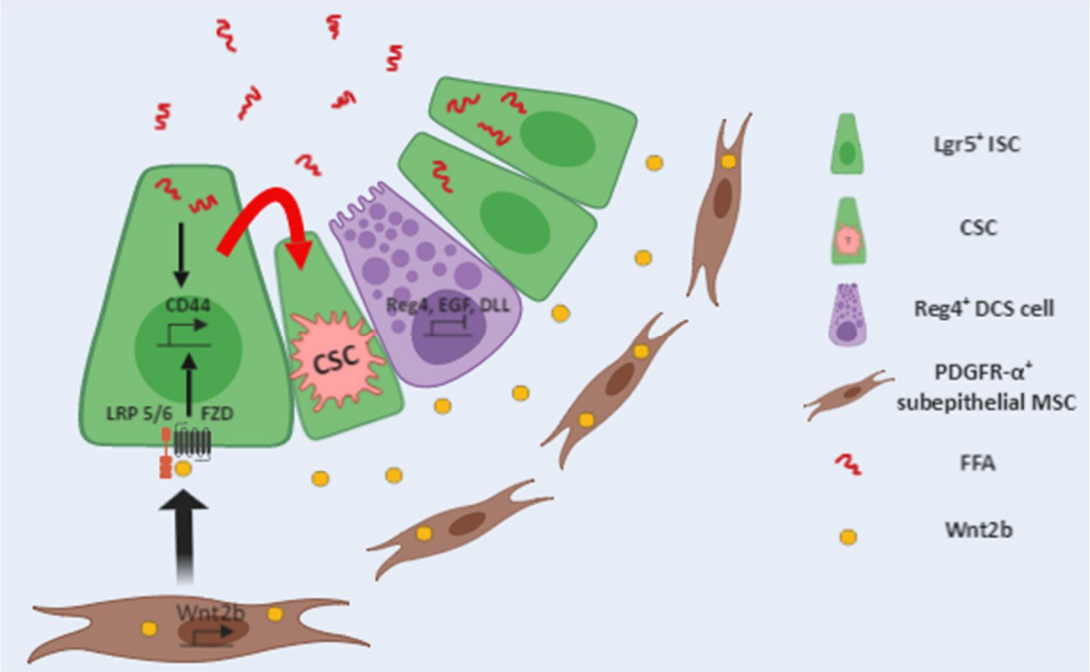

(Image was created with BioRender.com)

Reference

1. Clevers H. The intestinal crypt, a prototype stem cell compartment. Cell 2013;154:274-84.
2. Rodriguez-Colman MJ, Schewe M, Meerlo M, et al. Interplay between metabolic identities in the intestinal crypt supports stem cell function. Nature 2017;543:424-427.
3. Barker N, van Es JH, Kuipers J, et al. Identification of stem cells in small intestine and colon by marker gene Lgr5. Nature 2007;449:1003-7.
4. de Lau W, Peng WC, Gros P, et al. The R-spondin/Lgr5/Rnf43 module: regulator of Wnt signal strength. Genes Dev 2014;28:305-16.
5. Barriga FM, Montagni E, Mana M, et al. Mex3a marks a slowly dividing subpopulation of $Lgr5^+$ intestinal stem cells. Cell Stem Cell 2017;20:801-816 e7.
6. Barker N, Ridgway RA, van Es JH, et al. Crypt stem cells as the cells-of-origin of intestinal cancer. Nature 2009;457:608-11.
7. de Sousa e Melo F, Kurtova AV, Harnoss JM, et al. A distinct role for $Lgr5^+$ stem cells in primary and metastatic colon cancer. Nature 2017;543:676.
8. Gehart H, Clevers H. Tales from the crypt: new insights into intestinal stem cells. Nature Reviews Gastroenterology & Hepatology 2019;16:19-34.
9. Sato T, van Es JH, Snippert HJ, et al. Paneth cells constitute the niche for Lgr5 stem cells in intestinal crypts. Nature 2010;469:415.
10. Lee YS, Kim TY, Kim Y, et al. Microbiota-derived lactate accelerates intestinal stem-cell-mediated epithelial development. Cell Host Microbe 2018;24:833-846 e6.
11. Sasaki N, Sachs N, Wiebrands K, et al. $Reg4^+$ deep crypt secretory cells function as epithelial niche for $Lgr5^+$ stem cells in colon. Proceedings of the National Academy of Sciences 2016;113:E5399-E5407.
12. Farin HF, Van Es JH, Clevers H. Redundant sources of Wnt regulate intestinal stem cells and promote formation of paneth cells. Gastroenterology 2012;143:1518-1529 e7.

13. Kabiri Z, Greicius G, Madan B, et al. Stroma provides an intestinal stem cell niche in the absence of epithelial Wnts. Development 2014;141:2206-15.
14. Valenta T, Degirmenci B, Moor AE, et al. Wnt ligands secreted by subepithelial mesenchymal cells are essential for the survival of intestinal stem cells and gut homeostasis. Cell Rep 2016;15:911-918.
15. Mahida YR, Beltinger J, Makh S, et al. Adult human colonic subepithelial myofibroblasts express extracellular matrix proteins and cyclooxygenase-1 and -2. Am J Physiol 1997;273:G1341-8.
16. Sailaja BS, He XC, Li L. The regulatory niche of intestinal stem cells. J Physiol 2016;594:4827-36.
17. Shoshkes-Carmel M, Wang YJ, Wangensteen KJ, et al. Subepithelial telocytes are an important source of Wnts that supports intestinal crypts. Nature 2018;557:242-246.
18. Powell DW, Mifflin RC, Valentich JD, et al. Myofibroblasts. II. Intestinal subepithelial myofibroblasts. Am J Physiol 1999;277:C183-201.
19. Gong W, Guo M, Han Z, et al. Mesenchymal stem cells stimulate intestinal stem cells to repair radiation-induced intestinal injury. Cell Death &Amp; Disease 2016;7:e2387.
20. Stzepourginski I, Nigro G, Jacob J-M, et al. $CD34^+$ mesenchymal cells are a major component of the intestinal stem cells niche at homeostasis and after injury. Proceedings of the National Academy of Sciences 2017;114:E506-E513.
21. Degirmenci B, Valenta T, Dimitrieva S, et al. GLI1-expressing mesenchymal cells form the essential Wnt-secreting niche for colon stem cells. Nature 2018;558:449-453.
22. Koliaraki V, Pallangyo CK, Greten FR, et al. Mesenchymal cells in colon cancer. Gastroenterology 2017;152:964-979.
23. Anastas JN, Moon RT. Wnt signalling pathways as therapeutic targets in cancer. Nat Rev Cancer 2013;13:11-26.
24. Clevers H, Loh KM, Nusse R. Stem cell signaling. an integral program for tissue renewal and regeneration: Wnt signaling and stem cell control. Science 2014;346:1248012.

25. Zhan T, Rindtorff N, Boutros M. Wnt signaling in cancer. Oncogene 2016;36:1461.
26. Wang X, Wang X, Liu Y, et al. Lgr5 regulates gastric adenocarcinoma cell proliferation and invasion via activating Wnt signaling pathway. Oncogenesis 2018;7:57.
27. Valenta T, Gay M, Steiner S, et al. Probing transcription-specific outputs of beta-catenin in vivo. Genes Dev 2011;25:2631-43.
28. Voloshanenko O, Erdmann G, Dubash TD, et al. Wnt secretion is required to maintain high levels of Wnt activity in colon cancer cells. Nat Commun 2013;4:2610.
29. Igarashi M, Guarente L. mTORC1 and SIRT1 cooperate to foster expansion of gut adult stem cells during calorie restriction. Cell 2016;166:436-450.
30. Mihaylova MM, Sabatini DM, Yilmaz OH. Dietary and metabolic control of stem cell function in physiology and cancer. Cell Stem Cell 2014;14:292-305.
31. Yilmaz ÖH, Katajisto P, Lamming DW, et al. mTORC1 in the paneth cell niche couples intestinal stem-cell function to calorie intake. Nature 2012;486:490.
32. Beyaz S, Mana MD, Roper J, et al. High-fat diet enhances stemness and tumorigenicity of intestinal progenitors. Nature 2016;531:53-8.
33. Finucane MM, Stevens GA, Cowan MJ, et al. National, regional, and global trends in body-mass index since 1980: systematic analysis of health examination surveys and epidemiological studies with 960 country-years and 9.1 million participants. Lancet 2011;377:557-67.
34. Arkan MC, Hevener AL, Greten FR, et al. IKK-beta links inflammation to obesity-induced insulin resistance. Nat Med 2005;11:191-8.
35. Gulhane M, Murray L, Lourie R, et al. High fat diets induce colonic epithelial cell stress and inflammation that is reversed by IL-22. Sci Rep 2016;6:28990.
36. Dieleman LA, Palmen MJ, Akol H, et al. Chronic experimental colitis induced by dextran sulphate sodium (DSS) is characterized by Th1 and Th2 cytokines. Clin Exp Immunol 1998;114:385-91.
37. Andersson-Rolf A, Fink J, Mustata RC, et al. A video protocol of retroviral infection in primary intestinal organoid culture. J Vis Exp 2014:e51765.

38. Sato T, Stange DE, Ferrante M, et al. Long-term expansion of epithelial organoids from human colon, adenoma, adenocarcinoma, and Barrett's epithelium. Gastroenterology 2011;141:1762-72.

39. Sato T, Vries RG, Snippert HJ, et al. Single Lgr5 stem cells build crypt-villus structures in vitro without a mesenchymal niche. Nature 2009;459:262-5.

40. Koliaraki V, Kollias G. Isolation of intestinal mesenchymal cells from adult mice. Bio-protocol 2016;6:e1940.

41. Segata N, Izard J, Waldron L, et al. Metagenomic biomarker discovery and explanation. Genome Biol 2011;12:R60.

42. Dalby MJ, Ross AW, Walker AW, et al. Dietary uncoupling of gut microbiota and energy harvesting from obesity and glucose tolerance in mice. Cell Rep 2017;21:1521-1533.

43. Schulz MD, Atay C, Heringer J, et al. High-fat-diet-mediated dysbiosis promotes intestinal carcinogenesis independently of obesity. Nature 2014;514:508-12.

44. Turnbaugh PJ, Ley RE, Mahowald MA, et al. An obesity-associated gut microbiome with increased capacity for energy harvest. Nature 2006;444:1027-31.

45. Ley RE, Backhed F, Turnbaugh P, et al. Obesity alters gut microbial ecology. Proc Natl Acad Sci U S A 2005;102:11070-5.

46. Lee JC, Lee HY, Kim TK, et al. Obesogenic diet-induced gut barrier dysfunction and pathobiont expansion aggravate experimental colitis. PLoS One 2017;12:e0187515.

47. Everard A, Belzer C, Geurts L, et al. Cross-talk between *Akkermansia muciniphila* and intestinal epithelium controls diet-induced obesity. Proceedings of the National Academy of Sciences 2013;110:9066-9071.

48. Plovier H, Everard A, Druart C, et al. A purified membrane protein from *Akkermansia muciniphila* or the pasteurized bacterium improves metabolism in obese and diabetic mice. Nature Medicine 2016;23:107.

49. Zeilstra J, Joosten SP, Dokter M, et al. Deletion of the Wnt target and cancer stem cell marker CD44 in Apc(Min/+) mice attenuates intestinal tumorigenesis. Cancer Res 2008;68:3655-61.

50. Schmitt M, Metzger M, Gradl D, et al. CD44 functions in Wnt signaling by regulating LRP6 localization and activation. Cell Death And Differentiation 2014;22:677.

51. Nakano M, Kikushige Y, Miyawaki K, et al. Dedifferentiation process driven by TGF-beta signaling enhances stem cell properties in human colorectal cancer. Oncogene 2019;38:780-793.

52. Sahlberg SH, Spiegelberg D, Glimelius B, et al. Evaluation of cancer stem cell markers CD133, CD44, CD24: association with AKT isoforms and radiation resistance in colon cancer cells. PLoS One 2014;9:e94621.

53. Mani SA, Guo W, Liao MJ, et al. The epithelial-mesenchymal transition generates cells with properties of stem cells. Cell 2008;133:704-15.

54. Tsukamoto AS, Grosschedl R, Guzman RC, et al. Expression of the int-1 gene in transgenic mice is associated with mammary gland hyperplasia and adenocarcinomas in male and female mice. Cell 1988;55:619-25.

55. Fu L, Zhang C, Zhang LY, et al. Wnt2 secreted by tumour fibroblasts promotes tumour progression in oesophageal cancer by activation of the Wnt/beta-catenin signalling pathway. Gut 2011;60:1635-43.

56. Seo BR, Bhardwaj P, Choi S, et al. Obesity-dependent changes in interstitial ECM mechanics promote breast tumorigenesis. Sci Transl Med 2015;7:301ra130.

57. Isella C, Terrasi A, Bellomo SE, et al. Stromal contribution to the colorectal cancer transcriptome. Nat Genet 2015;47:312-9.

58. Tsujino T, Seshimo I, Yamamoto H, et al. Stromal myofibroblasts predict disease recurrence for colorectal cancer. Clin Cancer Res 2007;13:2082-90.

59. Alba-Castellón L, Olivera-Salguero R, Mestre-Farrera A, et al. Snail1-dependent activation of cancer-associated fibroblast controls epithelial tumor cell invasion and metastasis. Cancer Research 2016;76:6205-6217.

60. Ren Y, Jia HH, Xu YQ, et al. Paracrine and epigenetic control of CAF-induced metastasis: the role of HOTAIR stimulated by TGF-ss1 secretion. Mol Cancer 2018;17:5.

61. Wei L, Ye H, Li G, et al. Cancer-associated fibroblasts promote progression and gemcitabine resistance via the SDF-1/SATB-1 pathway in pancreatic cancer. Cell Death & Disease 2018;9:1065.

62. Pietras K, Pahler J, Bergers G, et al. Functions of paracrine PDGF signaling in the proangiogenic tumor stroma revealed by pharmacological targeting. PLoS Med 2008;5:e19.

63. Erez N, Truitt M, Olson P, et al. Cancer-associated fibroblasts are activated in incipient neoplasia to orchestrate tumor-promoting inflammation in an NF-kappaB-dependent manner. Cancer Cell 2010;17:135-47.

64. Mihaylova MM, Cheng CW, Cao AQ, et al. Fasting activates fatty acid oxidation to enhance intestinal stem cell function during homeostasis and aging. Cell Stem Cell 2018;22:769-778 e4.

국문 요약

식이에 의한 다양한 신호는 장 줄기세포의 증식과 이로 인한 종양형성을 조절하는 것으로 알려져 있다. 이전의 연구들은 고지방식이가 $Lgr5^+$ 장 줄기세포의 수를 증가시키고 대장암의 발생과 전이를 더욱 촉진한다는 것을 입증하였다. 그러나, 대장암 유발에 중요한 역할을 하는 것으로 알려진 장 줄기세포의 주변세포에는 고지방식이가 어떤 영향을 미치는지는 거의 알려져 있지 않다. 따라서 줄기세포의 주변세포에 대한 영향을 이해하는 것이 고지방식이에 의한 대장암 유발 기전을 규명하는 하나의 축이 될 것이다. 본 연구에서 정제된 대조 식이를 먹인 마우스와 비교하였을 때 고지방식이를 먹인 마우스의 대장에서 염증 지수가 증가하였으며, AOM-DSS 에 의한 대장암 유도도 유의적으로 증가시키는 것을 확인하였다. 비록 고지방식이를 먹인 마우스의 대장에서 장 줄기세포 수의 변화는 없었지만, 증식중인 $Ki67^+$ 세포는 유의적으로 증가하였다. 대장에서 장 줄기세포 분화를 돕는 주변세포 중 하나인 대장 중간엽 줄기세포의 기능에 초점을 맞추었다. 정제된 대조 식이를 먹인 마우스의 대장 중간엽 줄기세포와 비교했을 때 고지방식이를 먹인 마우스로부터 분리한 중간엽 줄기세포가 정상 대장 및 대장암 유래 오가노이드의 증식을 증가시켰다. 또한, 대장 유래 PDGFR-α^+ 중간엽 줄기세포에 의한 Wnt2b 분비가 고지방식이를 먹인 마우스에서 유의적으로 높았으며, 이는 중간엽 줄기세포가 식이에 의해 유도된 비만 마우스의 대장암 유발에 중요한 역할을 할 수 있음을 시사하였다. 장내세균총 분석 결과, 정제된 대조 식이를 먹인 마우스에 비해 고지방식이를 먹인 마우스의 대변에 존재하는 장내 세균의 다양성이 감소한 것으로 나타났다. 정제된 대조 식이를 먹인 마우스와 비교했을 때, 고지방식이를 먹인 마우스에서 맹장에서 유래된 짧은 사슬 지방산의 차이는 보이지 않은 반면에 유리 지방산의 양은 증가했다. 흥미롭게도 유리 지방산은 대장 오가노이드의 증식을 촉진시키는 데 중요한 역할을 하고 있었다. 이러한 결과는 식이 유래 비만에서 빈발하는 대장암 유발이 PDGFR-α^+ 중간엽 줄기세포 및 유리 지방산에 의한 대장암 줄기세포로의 분화 유도에 의한 것임을 시사하였다.

중심단어: 고지방식이, 대장암, 장 줄기세포, 중간엽 줄기세포